Quaternary Science Reviews 382 (2026) 109975

Contents lists available at ScienceDirect

Quaternary Science Reviews

journal homepage: www.elsevier.com/locate/quascirev

Sclerochemistry of archaeological mollusc shells from Inqitat (Dhofar, Oman): increasing seasonality and monsoon variability during the Late Holocene

Gaia Crippa [a,*], Andrea Chiari [a], Silvia Lischi [b,c], Mauro Cremaschi [a], Melanie J. Leng [d,e]

[a] Dipartimento di Scienze della Terra A. Desio, Università degli Studi di Milano, Via Mangiagalli 34, Milano, 20133, Italy
[b] Centre de Recherche Archéologique Jaussen & Savignac, University Paris 1 - Panthéon-Sorbonne, 3, rue Michelet, Paris, 75006, France
[c] CNRS - UMR 8167 «Orient & Méditerranée», 7, rue Guy Môquet, Villejuif, 94800, France
[d] National Environmental Isotope Facilities, British Geological Survey, Keyworth, Nottingham, NG12 5GG, UK
[e] Centre for Environmental Geochemistry, School of Biosciences, University of Nottingham, Loughborough, LE12 5RD, UK

ARTICLE INFO

Handling Editor: Dr Mira Matthews

Keywords:
Sclerochemistry
Archaeology
Seasonality
Monsoon
Iron age
Molluscs
Dhofar

ABSTRACT

Molluscs from archaeological contexts offer increasing potential for reconstructing past environments, climates, and human-environment interactions, particularly through the geochemical information archived in their shells. Here, we present the first sclerochemical analyses ($\delta^{18}O$, $\delta^{13}C$) conducted on Iron Age molluscs (9th century BCE – 1st century CE) from the Inqitat plateau in the Khor Rori Archaeological Park (Dhofar, Oman), with the aim of assessing changes in seasonal variability during the period of site occupation by the local population. Despite the abundance of archaeological shell assemblages, this region remains sclerochemically understudied due to its complex climatic and oceanographic setting. After selecting the best suitable shells and checking their preservation, we analysed ten specimens belonging to three species: the bivalves *Anadara uropigimelana* and *Tivela stefaninii*, and the gastropod *Oliva bulbosa*. Our results reveal an increase in seawater seasonality over the ~1000-year interval examined, from ~4 to ~8 °C, values exceeding the modern seasonal range along the Dhofar coast, with the most pronounced variability occurring in the last occupation phase. This enhanced seasonality likely reflects a progressive intensification of the summer monsoon and a strengthened upwelling of Indian Ocean waters along the Dhofar coast. Increased monsoon activity, particularly in the latest phase investigated, may have produced longer rainy seasons and more frequent flooding, prompting adaptive responses in the management of meteoric waters and flood-prone areas within the Khor Rori area and beyond. Nevertheless, coastal geomorphology, marine environmental conditions, and upwelling dynamics likely made the coastal area of Dhofar rich in food resources, thereby sustaining its attractiveness to past human communities.

1. Introduction

Mollusc shells are a common component of archaeological assemblages, as they are present in nearly all coastal environments that were inhabited or exploited by humans in the past (e.g., Prendergast and Stevens, 2014; Thomas, 2015). Indeed, shell-rich archaeological sites are widespread and occur globally, spanning diverse periods of human time (Thomas, 2015). Archaeological accumulations of mollusc shells are commonly found in middens and within settlements (e.g., Carenti and Wilkens, 2008; Gutiérrez-Zugasti, 2011; Gutiérrez-Zugasti et al., 2011; Prendergast and Stevens, 2014). While such mollusc deposits are typically interpreted as food refuse, coastal human populations also collected shells for a variety of other purposes, including their use as fish bait, in dye production, and as raw material for ornaments or tools (e.g., Lombardi et al., 2008; Campbell, 2017; Lischi, 2018, 2020).

Mollusc shells represent an increasingly valuable archive not only for understanding past human-environment interactions, but also for reconstructing past environmental changes either with traditional methods (based on species ecological and environmental requirements) or with geochemical analyses (Álvarez et al., 2011; Andrus, 2011; Thomas, 2015). In particular, the analysis of shell stable isotope compositions ($\delta^{18}O$, $\delta^{13}C$) using a sclerochemical approach – widely

* Corresponding author.
E-mail addresses: gaia.crippa@unimi.it (G. Crippa), andrea.chiari@unimi.it (A. Chiari), silvialischi@msn.com (S. Lischi), mauro.cremaschi@unimi.it (M. Cremaschi), mjl@bgs.ac.uk (M.J. Leng).

https://doi.org/10.1016/j.quascirev.2026.109975
Received 21 January 2026; Received in revised form 27 March 2026; Accepted 28 March 2026
Available online 2 April 2026
0277-3791/© 2026 The Authors. Published by Elsevier Ltd. This is an open access article under the CC BY license (http://creativecommons.org/licenses/by/4.0/).

employed in geological and modern contexts for seasonal (palaeo) environmental reconstructions – has been recently applied also to archaeological settings (e.g., Mannino et al., 2003; Andrus, 2011; Lindauer et al., 2017; Butler et al., 2019; García-Escárzaga et al., 2020; Schmitt et al., 2022). This high-resolution analysis offers a unique opportunity to characterise in detail past climatic and environmental changes and their effects on past human behaviours (Andrus, 2011; Twaddle et al., 2016), as well as determine the season of mollusc collection, contributing to the knowledge of ancient subsistence strategies and site occupation (e.g., Shackleton, 1973; Mannino et al., 2003, 2007; Burchell et al., 2013; Eerkens et al., 2013; Prendergast et al., 2016).

The environment plays a vital role in human life, providing the physical space and conditions within which populations operate (Twaddle et al., 2016). Consequently, changes in environmental conditions can act as powerful structuring agents, influencing human behaviour across multiple temporal and spatial scales (Rowland, 1983, 1999; Ulm, 2013; Twaddle et al., 2016). Understanding the environmental context in which past populations lived is therefore crucial for addressing key archaeological questions (Twaddle et al., 2016).

The oxygen isotope composition of mollusc shell carbonate primarily reflects the temperature and the isotopic composition of the water in which the organism lived (Epstein et al., 1953; Kim et al., 2007). In regions where environmental variability is driven predominantly by either temperature or water composition, establishing a causal relationship between isotopic signals from environment and carbonate is generally simple (Twaddle et al., 2016). However, in environments influenced by both temperature and variable water mixing (e.g., estuarine and freshwater systems or some tropical regions) disentangling these effects can be challenging, particularly when dealing with archaeological materials for which independent environmental data are lacking (Culleton et al., 2009; Andrus and Thompson, 2012; Twaddle et al., 2016). Some authors have even excluded material from such settings entirely, stating that their inherent complexities make them too difficult or inaccurate to analyse (e.g. Godfrey, 1988; Milner, 2001; Twaddle et al., 2016). As a result, research often concentrates on organisms and habitats that are less affected by fluctuations in seawater $\delta^{18}O$ values (Andrus, 2011). Nevertheless, a growing body of research has demonstrated the efficacy of using oxygen isotopes even in regions characterised by more complex temperature-water composition dynamics, particularly when combined with high-resolution growth feature analysis, modern comparative baselines or additional stable isotope analysis (e.g., Kennett and Voorhies, 1995; Kirby et al., 1998; Andrus and Crowe, 2000; Surge et al., 2001; Jones et al., 2005; Twaddle et al., 2016; Caldarescu et al., 2021; de Winter et al., 2024).

In this study, we performed sclerochemical analyses on mollusc specimens belonging to three different species, the bivalves *Anadara uropigimelana* (Bory de St.-Vincent, 1827) and *Tivela stefaninii* (Nardini, 1933), and the gastropod *Oliva bulbosa* (Röding, 1798.), collected from a climatic and oceanographic complex setting in the Dhofar Governorate, southern Oman. These species are commonly found in archaeological shell assemblages of the Arabian Peninsula (e.g., Martin, 2005; Roselló-Izquierdo et al., 2005; Lindauer et al., 2017, 2018; Callapez and Dinis, 2020; Crippa et al., 2024) and are currently living in the Indo-Pacific region (e.g., Tursch and Germain, 1985; Lutaenko, 2011; Grizzle et al., 2018). Their abundance in archaeological contexts, combined with the presence of clear growth lines and increments in their shells, makes them excellent archives for high resolution palaeoclimatic and palaeoenvironmental reconstructions.

The examined molluscs come from Iron Age circular houses within the HAS1 settlement and from an adjacent midden, located on the Inqitat plateau (Khor Rori Archaeological Park), a site characterised by abundant mollusc remains (Crippa et al., 2024). This site is of fundamental importance for understanding the indigenous population of the area and their habits. Discovered in 2016, it has since then been the subject of extensive investigation by the DHOMIAP Project, focusing on its characteristics, chronology and interactions with the nearby South Arabian city of Sumhuram (Lischi, 2019a, 2019b, 2021, 2023). A recent multimethodological study by Crippa et al. (2023) on both burned and unburned mollusc shells from the circular houses and supported by on-site observations, suggests that the HAS1 settlement was completely destroyed by a fire. This event appears to have led to the abandonment of the promontory by local inhabitants belonging to the Dhofar Coastal Culture.

The present study is the first to deal with a sclerochemical analyses of Iron Age molluscs in the Dhofar region, and the first to focus on the three species examined here. Most published research on archaeological molluscs from Oman is geographically and chronologically distant from the context under investigation. To our knowledge, only a few studies have addressed the sclerochemistry of archaeological molluscs from Oman. Martin (2005) investigated marine molluscs from Neolithic to Bronze Age sites in the Ja'alan region (northern Oman); Berger et al. (2020) briefly analysed marine bivalves from the Neolithic site of Ruways-1 (northern Oman), and Schmitt et al. (2022) studied aquatic and terrestrial gastropods from the Al-Khashbah site, dated to the Early Bronze Age and the Late Islamic Period, in northern Oman. The present study investigates the palaeoclimatic conditions prevailing during a selected interval of settlement occupation (9th century BCE – 1st century CE), employing mollusc shells as archives of seasonality, to infer seasonal seawater temperature fluctuations, evaluate the long-term variability in seasonal climate patterns and understand how these changes affect the population behaviour.

2. Geological and geomorphological setting

The HAS1 settlement is situated on the Inqitat promontory on the eastern side of the Wadi Darbāt estuary, within the Khor Rori Archaeological Park about 40 km east of Salalah, in the Dhofar Governorate, southern Oman (Fig. 1A and B).

The mouth of Wadi Darbāt is flanked by two promontories located on either side (east and west), known by several names, including Inqitat Mirbat and Inqitat Taqah, al-Hamr al Sharqiya (which gives the settlement its acronym HAS1) and al-Hamr al Wusta, or al Humr al Tarfiyah and al Humr al Wusta. These promontories are mesas of a broader marine erosional terrace extending from Taqah to the Wadi Hinna valley near Mirbat. This marine terrace ranges in elevation from 30 to 100 m above sea level and is limited seaward by a steep scarp. Although no direct dating has been conducted, the terrace is thought to have formed during the Late Pleistocene (MIS 5; Cremaschi, 1996, 2017; Cremaschi and Negrino, 2002; Hoorn and Cremaschi, 2004).

The eastern Inqitat's geological bedrock consists of Oligocene shallow-marine and shoreline bioclastic and micritic limestone, belonging to the Ashawq Formation (Roger et al., 1989), and immerging to the S–SE in the seaward direction. They are unconformably cut to the top by a Pleistocene erosional surface, which forms the flat surface of the Inqitat. A valley runs through the middle part of the mesa, dividing the Inqitat into two parts in the east–west direction.

Its formation is due to the presence of systems of normal faults, which have amplified the effect of the erosional processes that fragmented the Pleistocene marine terrace into two distinct mesas, now known as the Inqitat promontories. These erosional processes were most active during the Last Glacial Maximum (~20 ka), driven by a significant drop in the sea level (Hoorn and Cremaschi, 2004; Cremaschi, 2017; Zerboni et al., 2020).

The surface of the Inqitat is covered by a palaeosol of the terra rossa type characterised by a red colour, a clayey texture, and the presence of carbonate and gypsum concretions. The palaeosol, developed on the marine abrasion terrace during MIS 5 and reflects a long history of climatic fluctuations, indicating a period in the past marked by greater water availability and a dense vegetal cover (Cremaschi and Perego, 2008; Cremaschi, 2017).

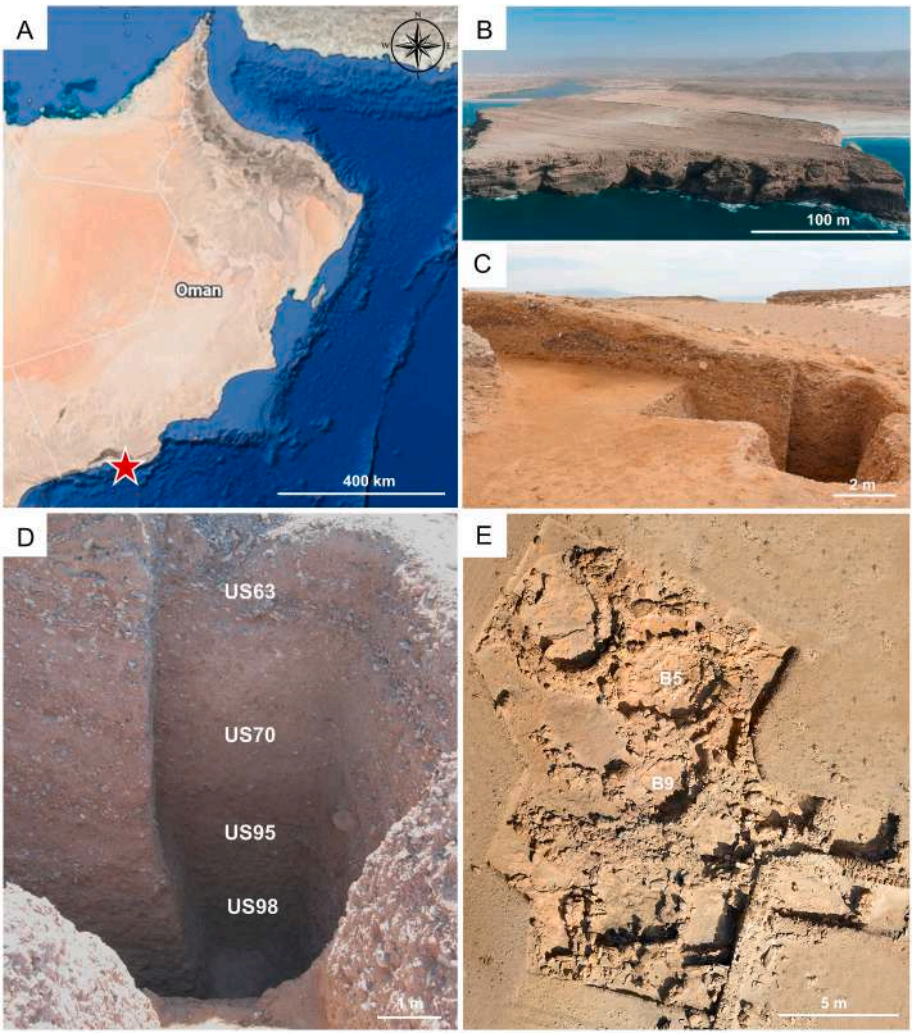

Fig. 1. A) Location of the Inquitat plateau in the Dhofar region, Oman (red star). B) Northern plateau of the Inqitat promontory where the HAS1 settlement is situated. C) Part of the eastern section of the midden with the trench, where specimens from US63, US70, US95 come from. D) Detail of the trench in the midden showing the alternation of layers and the sampled stratigraphic units. E) HAS1 settlement showing the position of the circular structures (B5, B9), where specimens from US30 and US54 come from.

3. Materials

Ten mollusc specimens belonging to three different species were here analysed: two bivalves, *Anadara uropigimelana* and *Tivela stefaninii*, and one gastropod, *Oliva bulbosa*. All the specimens are currently housed in the collections of the Dipartimento di Scienze della Terra 'A. Desio' of the University of Milan and registered with reference numbers consisting of a prefix MPUM followed by a five-digit number (Table 1). Field numbers are used for simplicity when referring to the specimens in the text (Table 1).

Anadara uropigimelana is an epifaunal/seminfaunal species living in muddy, sandy or rocky substrates in intertidal-infralittoral settings, *Tivela stefaninii* is an infaunal bivalve of sandy intertidal to infralittoral settings, whereas *Oliva bulbosa* is an epifaunal gastropod living mainly in muddy-sandy to sandy intertidal-shallow infralittoral settings (Crippa et al., 2024 and refs therein).

Mollusc specimens come from two different areas on the Inqitat plateau, Khor Rori, Oman (17°01′45.2″ N, 54°26′32.4″ E): the HAS1 settlement, located in the centre of the northern plateau of Inqitat, and the trash dump or midden, located on the northern side of the intermediate valley of Inqitat (Fig. 1A and B). The settlement is composed of circular or semi-circular megalithic structures, used as houses. They are formed by a stone basement made by a sandwich wall, filled with soil mixed with rocks of different sizes, and by a not preserved roof probably constituted by perishable material and supported by wooden poles. A multimethodological study on burned and unburned mollusc shells from the HAS1 circular structures (Crippa et al., 2023) and traces of the poles and the roof found carbonised *in situ* during the excavation activities (Lischi, 2019a; 2023), indicated that the site was engulfed by a fire. The northern cliff of the intermediate valley is characterised by a series of middens with a conical shape and significant volume (Cremaschi and Perego, 2008; Lischi, 2023, 2026); one of these has been stratigraphically sampled through an excavated trench nearly 4 m deep.

The specimens here examined were collected from two stratigraphic units within two circular structures (circular structures B5, US30 and B9, US54) and from three stratigraphic units within the excavated midden (US63, US70, US95) (Fig. 1C–E). The stratigraphic unit US30 is the lowest layer found in the circular structure B5, being composed of big fragments of charcoal mixed with medium and small stones, completely carbonised wooden poles and complete vessels (Crippa et al., 2024). The stratigraphic unit US54 is found inside the circular structure B9; here carbonised wooden beams and a lot of fire traces (charcoals) occur, together with some archaeological materials, suggesting the contemporaneity with US30 (Lischi, 2019a, 2022, 2023). In the midden, three stratigraphic units have been sampled: US63 is the shallower one, followed by US70 and US95 going deeper in the trench (Fig. 1 D). This long

Table 1
Specimens analysed for sclerochemistry. For each specimen are reported the stratigraphic unit (US) from which the specimen come from, the ID number, the museum number (MPUM), the species name and the age of each stratigraphic unit based on radiocarbon dating, as well as the subdivision of the stratigraphic units into Phase 1, 2 and 3.

	US	ID number		MPUM number	Species	Age
Phase 3	US30	T2	BS-246	12340	*Tivela stefaninii*	1st century CE
		O3	BS-49	12409	*Oliva bulbosa*	
	US54	A4	OS-107	12335	*Anadara uropigimelana*	
		T3	OS-120	12341	*Tivela stefaninii*	
Phase 2	US63	A3	MS-296	12336	*Anadara uropigimelana*	515 – 349 cal BCE
		O1	MS-24	12411	*Oliva bulbosa*	
	US70	A2	A2	12337	*Anadara uropigimelana*	702 – 397 cal BCE
		T1	T1	12343	*Tivela stefaninii*	
Phase 1	US95	A1	A1	12338	*Anadara uropigimelana*	Intermediate between US70 and US98
		O2	OB1	12413	*Oliva bulbosa*	
	US98			Not sampled		843 – 739 cal BCE

stratigraphy stretches from the beginning to the end of the Iron Age (9th century BCE to 1st century CE).

The HAS1 settlement (Meghalayan, Late Holocene) was inhabited from at least the 4th century BCE until the 1st-2nd century CE (Middle-Late Iron Age) (Lischi, 2018; 2019a; 2022, 2023). Based on radiocarbon dating on animal bones and charcoal the stratigraphic units here investigated show the following ages (Lischi, 2019a): US70 (702 – 397 cal BCE), US63 (515 – 349 cal BCE), US30 (1st century CE) (Table 1). US54 and US95 have not been dated, but US54 is coeval with US30, and US95 has an intermediate position between US70 and US98 (843 – 739 cal BCE), and thus an intermediate age (Table 1).

These stratigraphic units correspond to three distinct occupation phases of the promontory by the local populations, as identified by the stratigraphic analysis, by the material culture recovered during the excavation (Lischi, 2022) and by the exploitation of the resources (e.g., molluscs, Crippa et al., 2024). From the oldest to the youngest the following phases were identified: (1) Phase 1, US95 and US98 (Early Iron Age, 1200–800 BCE), (2) Phase 2, US63 and US70 (Middle Iron Age, 800–300 BCE), and (3) Phase 3, US30 and US54 (Late Iron Age, 300 BCE–300 CE).

4. Methods

Ten specimens were analysed for sclerochemical analyses ($\delta^{13}C$, $\delta^{18}O$): four specimens of *Anadara uropigimelana*, three specimens of *Tivela stefaninii* and three specimens of *Oliva bulbosa*. For each stratigraphic unit two shells belonging to two different species were selected (Table 1).

Prior to isotope analyses, shells were checked for preservation through Scanning Electron Microscopy and X-Ray Powder Diffraction analyses. The results of these analyses are reported in Chiari et al. (2025), where a detailed description of the mineralogy and of the microstructure is provided together with the sample preparation procedure of each analysis. All the shells are well-preserved showing the original microstructure and aragonite mineralogy.

For sclerochemical analyses, bivalve specimens were sectioned longitudinally from the umbo to the ventral region along the axis of maximum growth using a low speed saw with a thin diamond blade, whereas gastropod specimens were cut transversally, perpendicular to the growth axis; subsequently, 5 mm-thick slices were cut from each half specimen to obtain two specular sections for each specimen and mounted on glass slides. These sections were smoothed with 400 and 1000 grit SiC powder and cleaned with demineralized water. One section was prepared for SEM analysis following the procedure of Crippa et al. (2016), whereas the other section was polished with 1 μm Al_2O_3 to make the growth lines clearer. The polished section was first photographed using a Motic SMZ-171-TLed stereomicroscope at 7.5x magnification. Multiple images were taken for each specimen and combined using the "Photomerge command" tool in Adobe Photoshop (Adobe Inc.) to create a high-resolution image of the shell, allowing clear visualization of the growth lines.

The polished section was then sampled at high resolution (~1 mm spacing) using a microdrill (Dremel 3000) equipped with a 300-μm tungsten carbide drill bit. Bivalve shells were sampled from the dorsal to the ventral margin when the entire shell was preserved, whereas gastropod shells were sampled only in the last years of growth, where the outer shell layer was thicker, from nearly mid-shell toward the shell aperture. The number of powder samples collected from each specimen was variable, from 17 to 52 samples per shell, covering different years of shell growth (Supplementary Fig. S1). We collected from a minimum of 7 (in *Oliva bulbosa*) to a maximum of 41 samples (in *Anadara uropigimelana*) per year. Assuming an approximately constant shell growth, we collected samples with a roughly bimonthly to nearly weekly resolution. Although the precise age of each individual sample cannot be constrained, the sampling density is sufficient to resolve the seasonal cycle and identify annual temperature maxima and minima.

For isotope analyses c. 50 μg of carbonate were dissolved in 100% phosphoric acid and the carbon and oxygen isotope ratios ($^{13}C/^{12}C$ and $^{18}O/^{16}O$) were measured using an Isoprime dual inlet mass spectrometer plus Multiprep device at the British Geological Survey, Keyworth (UK). Isotope values ($\delta^{13}C$, $\delta^{18}O$) are reported as per mil (‰) deviations of the isotope ratios calculated to the V-PDB scale using a within-run laboratory standard (KMC) calibrated against the international standards (NBS18 and NBS19). Analytical reproducibility for these analyses was better than 0.1‰ for $\delta^{13}C$ and $\delta^{18}O$.

Seawater temperature seasonality was estimated using two approaches (Table 2): method 1) by calculating the difference between the maximum and minimum $\delta^{18}O$ values ($\delta^{18}O_{max\text{-}as}$, $\delta^{18}O_{min\text{-}as}$) recorded across the entire shell ($\Delta\delta^{18}O_{as}$), which reflects the maximum seasonality captured in the sampled interval by each shell; and method 2) by identifying the larger amplitude $\delta^{18}O$ cycle ($\Delta\delta^{18}O_{oc}$) calculated as the difference between the maximum and minimum $\delta^{18}O$ values ($\delta^{18}O_{max\text{-}oc}$, $\delta^{18}O_{min\text{-}oc}$) within a single cycle, defined between two consecutive annual growth lines. We here refer to seasonality as the difference between maximum and minimum isotope values, corresponding to the difference between the warmest and coldest seawater temperatures (Kwiecien et al., 2022). In using both methods, we capture the maximum seasonality experienced by the organism during its life/sampled interval (method 1) and the maximum seasonality experienced by the organism in one year (method 2). We acknowledge that estimates of seasonality based on T_{max}–T_{min} can be sensitive to temporal resolution, as higher-resolution records may, in some cases, increase the likelihood of capturing extreme values. At the same time, this approach allows to capture the full amplitude of the seasonal cycle recorded in the shell, including short-lived extremes that may be ecologically and climatically relevant. However, in sclerochemical records, the relationship between recorded values and environmental extremes is further complicated by biological factors such as variable growth rates and seasonal growth cessation. Therefore, given the high-resolution but non-continuous sampling strategy and the possibility of species-specific shell growth

Table 2
Stable isotope results. For each analysed specimen are reported the Phase, the US, the ID number, the species, the maximum and minimum $\delta^{18}O$ values ($\delta^{18}O_{max}$, $\delta^{18}O_{min}$), the difference between the maximum and minimum values ($\Delta\delta^{18}O$) and the corresponding palaeotemperature values (T_{max}, T_{min}, ΔT) for the all shell ($_{as}$) and for one cycle (i.e., the larger amplitude cycle) ($_{oc}$).

	US	ID number	Species	$\delta^{18}O_{max\text{-}as}$ (‰)	$T_{min\text{-}as}$ (°C)	$\delta^{18}O_{min\text{-}as}$ (‰)	$T_{max\text{-}as}$ (°C)	$\Delta\delta^{18}O_{as}$ (‰)	ΔT_{as} (°C)
Phase 3	US30	T2	*Tivela stefaninii*	−0.38	23.25	−2.39	31.97	2.01	8.72
		O3	*Oliva bulbosa*	+0,15	20.95	−1.08	26.29	1.23	5.34
	US54	A4	*Anadara uropigimelana*	+0,20	20.73	−1.85	29.63	2.05	8.90
		T3	*Tivela stefaninii*	+1,05	17.04	−1.62	28.63	2.67	11.59
Phase 2	US63	A3	*Anadara uropigimelana*	+0,19	20.77	−1.56	28.37	1.75	7.60
		O1	*Oliva bulbosa*	+0,69	18.60	−0.2	22.47	0.89	3.87
	US70	A2	*Anadara uropigimelana*	−0.02	21.69	−1.28	27.15	1.26	5.46
		T1	*Tivela stefaninii*	−0.16	22.29	−1.85	29.63	1.69	7.34
Phase 1	US95	A1	*Anadara uropigimelana*	−0.25	22.68	−1.41	27.72	1.16	5.04
		O2	*Oliva bulbosa*	+0,12	21.08	−0.94	25.68	1.06	4.60
	US	**ID number**	**Species**	**$\delta^{18}O_{max\text{-}oc}$ (‰)**	**$T_{min\text{-}oc}$ (°C)**	**$\delta^{18}O_{min\text{-}oc}$ (‰)**	**$T_{max\text{-}oc}$ (°C)**	**$\Delta\delta^{18}O_{oc}$ (‰)**	**ΔT_{oc} (°C)**
Phase 3	US30	T2	*Tivela stefaninii*	−0.54	23.94	−2.39	31.97	1.85	8.03
		O3	*Oliva bulbosa*	+0,13	21.03	−1.08	26.29	1.21	5.26
	US54	A4	*Anadara uropigimelana*	+0,20	20.73	−1.85	29.63	2.05	8.90
		T3	*Tivela stefaninii*	+1,05	17.04	−1.22	26.89	2.27	9.85
Phase 2	US63	A3	*Anadara uropigimelana*	+0,15	20.95	−1.56	28.37	1.71	7.42
		O1	*Oliva bulbosa*	+0,69	18.60	−0.05	21.82	0.74	3.22
	US70	A2	*Anadara uropigimelana*	−0.02	21.69	−1.28	27.15	1.26	5.46
		T1	*Tivela stefaninii*	−0,16	22.29	−1.56	28.34	1.40	6.05
Phase 1	US95	A1	*Anadara uropigimelana*	−0,43	23.46	−1.41	27.72	0,98	4.26
		O2	*Oliva bulbosa*	+0,12	21.08	−0.48	23.68	0.60	2.60

cessation when temperatures are at their extremes, we cannot exclude the possibility that some absolute seasonal extremes were not captured, meaning that the reconstructed amplitude of seasonality could represent a minimum estimate.

For each shell, the maximum ($\delta^{18}O_{max}$), minimum ($\delta^{18}O_{min}$) and average ($\delta^{18}O_{avg}$) $\delta^{18}O$ values were also determined (Tables 2 and 3).

For all $\delta^{18}O$ values (maximum, minimum, average) and $\delta^{18}O$ variations ($\Delta\delta^{18}O$) we calculated the corresponding maximum ($T_{max\text{-}as}$, $T_{max\text{-}oc}$), minimum ($T_{min\text{-}as}$, $T_{min\text{-}oc}$) and average (T_{avg}) palaeotemperatures, as well as palaeotemperature excursions (ΔT_{as}, ΔT_{oc}) using the modified equation of Grossman and Ku (1986) (Tables 2 and 3). Since no direct data for the $\delta^{18}O$ value of seawater ($\delta^{18}O_{sw}$) are available for the studied time interval in the Dhofar region, $\delta^{18}O_{sw}$ was assumed to be equal to the present-day value for the area (+0,5 ‰) (Schmidt et al., 1999).

Data on annual salinity variation in the area are scarce. Tudhope et al. (1996) indicate that seasonal salinity differences off Southern Oman are typically less than 0,4 ‰, while Shahjahan et al. (2012, their Fig. 7) reported no significant salinity variation in shallow waters (5 m) at Salalah between summer and winter. If we consider a salinity annual variability of 0,4 ‰, this would correspond to an estimated $\delta^{18}O_{sw}$ variability of approximately 0,1 ‰ using the surface $\delta^{18}O_{sw}$-salinity relationship of Delaygue et al. (2001) for the Arabian Sea. Such variability would translate into temperature uncertainties of <0,5 °C.

The seasonal amplitude recorded by mollusc specimens, reconstructed subtracting the minimum temperature from the maximum temperature derived from sequential isotopic sampling of the shell, was compared to the modern seasonal temperature range, calculated with the same approach as the difference between the maximum and minimum seawater temperature, using data obtained from website (weatherspark.com) and other sources related to nearby areas (e.g. Prell and Streeter, 1982; Tudhope et al., 1996; Khan et al., 2021). We acknowledge that modern datasets are based on multi-year monthly averages, whereas shell-based values reflect discrete sampling points along the growth profile. Because both modern and fossil seasonality values represent single seasonal amplitudes (i.e., ranges defined as $T_{max}-T_{min}$) a formal statistical comparison was not applied. The comparison is therefore descriptive and aims to evaluate differences in absolute seasonal amplitude between fossil shells and modern conditions.

As previously discussed, the stratigraphic units examined correspond to three distinct occupation phases of the promontory by the local populations (Table 1). To facilitate the comparison between these phases and to identified potential trends, we also estimated the average palaeotemperature ($T_{avg\text{-}phase}$) and the average palaeotemperature excursion ($\Delta T_{avg\text{-}as}$, $\Delta T_{avg\text{-}oc}$) for each phase. These were calculated by averaging the average palaeotemperatures and the palaeotemperature excursions recorded by each species (both across the entire shell and within the main cycle) within each phase (Table 3). Similarly, we determined the average $\delta^{18}O$ values for warm and cold intervals ($\delta^{18}O_{avg\text{-}warm}$, $\delta^{18}O_{avg\text{-}cold}$) and their corresponding palaeotemperatures ($T_{avg\text{-}warm}$, $T_{avg\text{-}cold}$) for each occupation phase (Table 3).

For each shell, the maximum ($\delta^{13}C_{max}$), minimum ($\delta^{13}C_{min}$) and $\Delta\delta^{13}C$ values were also determined for the entire shell and the larger amplitude cycle, as well as the average value ($\delta^{13}C_{avg}$) (Table 4).

5. Results

5.1. Growth lines

The microstructure of growth lines in the three examined species at the SEM have already been extensively described by Chiari et al. (2025); here, we report only the key features relevant to the discussion.

The shell of *Anadara uropigimelana* is characterised by major and minor growth lines (Fig. 2). In polished sections, these appear as thin, slightly darker (light grey) bands alternating with lighter ones, representing growth increments. On the outer shell surface major annual growth lines form prominent steps (Fig. 2A and B). Between major growth lines, numerous thin minor growth lines occur on the shell surface, mainly observable in the interspaces between the costae. At the SEM the growth line microstructure is generally well-defined and consists of irregular simple prisms; in some cases, however, the prisms are less distinct and growth lines correspond to bands of higher porosity (Fig. 2C–E). Growth lines cross both outer and inner layers. In the outer layer major growth lines cross only the crossed lamellar microstructure, but not the dendritic non denticular composite prismatic one.

Numerous major and minor growth lines cross the shell of *Tivela stefaninii*. In polished sections, they appear as darker bands alternating with lighter ones, corresponding to growth increments. The darker bands may be thin and distinct, or thicker and more diffuse, often consisting of a bundle of several growth lines (Fig. 3A). Occasionally, they form small steps on the outer shell surface; more often, the latter is

Table 3
Stable isotope results. For each analysed specimen are reported the Phase, the US, the ID number, the species and the average $\delta^{18}O$ and temperature values ($\delta^{18}O_{avg}$, T_{avg}). The average temperature ($T_{avg\text{-}phase}$), the average coldest and warmest temperatures ($T_{avg\text{-}warm}$, $T_{avg\text{-}cold}$) and the average seasonal temperature variation for the all shell and one cycle ($\Delta T_{avg\text{-}as}$, $\Delta T_{avg\text{-}oc}$) in each occupation phase are also provided, as well as the average $\delta^{18}O$ values of the highest and lowest $\delta^{18}O$ values ($\delta^{18}O_{avg\text{-}warm}$, $\delta^{18}O_{avg\text{-}cold}$).

	US	ID number	Species	$\delta^{18}O_{avg}$ (‰)	T_{avg} (°C)	$T_{avg\text{-}phase}$ (°C)	$\delta^{18}O_{avg\text{-}warm}$ (‰)	$T_{avg\text{-}warm}$ (°C)	$\delta^{18}O_{avg\text{-}cold}$ (‰)	$T_{avg\text{-}cold}$ (°C)	$\Delta T_{avg\text{-}as}$ (°C)	$\Delta T_{avg\text{-}oc}$ (°C)
Phase 3	US30	T2	*Tivela stefaninii*	−1.14	26.55	24.76	−1.74	29.13	+0,26	20.49	8.64	8.01
		O3	*Oliva bulbosa*	−0.45	23.55							
	US54	A4	*Anadara uropigimelana*	−0.91	25.55							
		T3	*Tivela stefaninii*	−0.41	23.38							
Phase 2	US63	A3	*Anadara uropigimelana*	−0.45	23.55	23.75	−1.22	26.91	+0,18	20.84	6.07	5.54
		O1	*Oliva bulbosa*	+0,21	20.69							
	US70	A2	*Anadara uropigimelana*	−0.72	24.72							
		T1	*Tivela stefaninii*	−1.02	26.03							
Phase 1	US95	A1	*Anadara uropigimelana*	−0.71	24.68	24.27	−1.18	26.70	−0.07	21.88	4.82	3.43
		O2	*Oliva bulbosa*	−0.52	23.86							

crossed by numerous growth lines of similar size. Distinguishing between major and minor growth lines is not always straightforward. At the SEM, the microstructure of the growth lines is generally composed of irregular simple prisms. However, this microstructure is not always clearly visible; indeed, in some cases, growth lines are recognizable due to their different brightness with respect to the surrounding layer. Looking in more detail, these growth lines are associated with an increase in the size and a change in the shape of the basic structural units, forming an aligned row of small prisms; this often coincides with the presence of a thin band of higher porosity (Fig. 3B–E).

The shell of *Oliva bulbosa* is crossed by major and minor growth lines. In polished sections, major annual growth lines appear as darker bands alternating with lighter ones, corresponding to growth increments. These major lines cross the outer and middle layer, interrupting the transitional layer, which appears as a thin, white layer in the central part of the shell section (Fig. 4 A). On the outer shell surface major growth lines appear as shallow grooves. At the SEM, growth lines in the outer and middle layers are curved, following the outline of the aperture (Fig. 4 B), whereas in the inner layer they are parallel to the external and internal shell surfaces. The microstructure of major growth lines consists of a stockade of irregular simple prisms (Fig. 4C and D). Numerous minor growth lines occur within the transitional layer, not extending into the outer and middle layers (Fig. 4E and F). The microstructure of minor growth lines is often unclear; they are typically visible due to their different brightness compared to the surrounding layer and are frequently associated with thin bands of higher porosity (Fig. 4 F).

5.2. Stable isotopes

The results of stable isotope analyses (Figs. 5–7) show that annual growth lines in the *A. uropigimelana* specimens here analysed generally record the highest $\delta^{13}C$ and $\delta^{18}O$ values. The correlation between annual growth lines and isotope profiles is not straightforward in the *T. stefaninii* specimens here analysed. Growth lines generally record intermediate $\delta^{18}O$ values, between the lowest and highest $\delta^{18}O$ values, with no clear correspondence with $\delta^{13}C$ values. Annual growth lines in the *O. bulbosa* specimens here examined record in many cases the lowest $\delta^{18}O$ values, with no particular correlation with $\delta^{13}C$ values.

The stable isotope results are hereafter presented divided by the three occupation phases of the settlement by the local population and are reported in Figs. 5–8 and Tables 2–4. Measured $\delta^{13}C$ and $\delta^{18}O$ values of each shell sample are reported in the Supplementary Material (Table S1).

In the oldest phase (Phase 1) two specimens were analysed belonging to *Anadara uropigimelana* (A1) and *Oliva bulbosa* (O2) (Fig. 5). Considering the entire shell, the ΔT_{as} ranges from 4,60 °C (*O. bulbosa*) to 5,04 °C (*A. uropigimelana*) (Fig. 8A–Table 2). Considering one cycle, the ΔT_{oc} ranges from 2,60 °C (*O. bulbosa*) to 4,26 °C (*A. uropigimelana*) (Fig. 8B–Table 2). The $\Delta\delta^{13}C_{as}$ and $\Delta\delta^{13}C_{oc}$ values range from 0,73 ‰ (*O. bulbosa*) to 1,44 ‰ (*A. uropigimelana*) and from 0,70 ‰ (*O. bulbosa*) to 1,44 ‰ (*A. uropigimelana*), respectively (Table 4).

In the middle phase (Phase 2) four specimens were analysed: two shells of *A. uropigimelana* (A2, A3), one of *T. stefaninii* (T1) and one of *O. bulbosa* (O1) (Fig. 6). Considering the entire shell, the ΔT_{as} ranges from 3,87 °C (*O. bulbosa*) to 7,60 °C (*A. uropigimelana*) (Fig. 8A–Table 2). Considering one cycle, the ΔT_{oc} ranges from 3,22 °C (*O. bulbosa*) to 7,42 °C (*A. uropigimelana*) (Fig. 8B–Table 2). The $\Delta\delta^{13}C_{as}$ and $\Delta\delta^{13}C_{oc}$ values range from 1,12 ‰ (*T. stefaninii*) to 1,95 ‰ (*A. uropigimelana*) and from 0,90 ‰ (*O. bulbosa*) to 1,87 ‰ (*A. uropigimelana*), respectively (Table 4).

In the youngest phase (Phase 3) four specimens were analysed: one shell of *A. uropigimelana* (A4), two of *T. stefaninii* (T2, T3) and one of *O. bulbosa* (O3) (Fig. 7). Considering the entire shell, the ΔT_{as} ranges from 5,34 °C (*O. bulbosa*) to 11,39 °C (*T. stefaninii*) (Fig. 8A–Table 2). Considering one cycle, the ΔT_{oc} ranges from 5,26 °C (*O. bulbosa*) to

Table 4
Stable isotope results. For each analysed specimen are reported the US, the ID number, the species, the maximum and minimum $\delta^{13}C$ values ($\delta^{13}C_{max}$, $\delta^{13}C_{min}$), the difference between the maximum and minimum values ($\Delta\delta^{13}C$) for the all shell ($_{as}$) and for one cycle (i.e., the larger amplitude cycle) ($_{oc}$), as well as the average $\delta^{13}C$ value ($\delta^{13}C_{avg}$).

US	ID number	Species	$\delta^{13}C_{max\text{-}as}$ (‰)	$\delta^{13}C_{min\text{-}as}$ (‰)	$\Delta\delta^{13}C_{as}$ (‰)	$\delta^{13}C_{max\text{-}oc}$ (‰)	$\delta^{13}C_{min\text{-}oc}$ (‰)	$\Delta\delta^{13}C_{oc}$ (‰)	$\delta^{13}C_{avg}$ (‰)
US30	T2	*Tivela stefaninii*	+1,96	−0,72	2,68	+1,23	−0,72	1,95	+0,59
	O3	*Oliva bulbosa*	+1,86	+1,27	0,59	+1,86	+1,49	0,37	+1,58
US54	A4	*Anadara uropigimelana*	+0,17	−1,00	1,17	+0,17	−1,00	1,17	−0,50
	T3	*Tivela stefaninii*	+1,76	+0,72	1,04	+1,67	+0,73	0,94	+1,25
US63	A3	*Anadara uropigimelana*	+0,90	−1,05	1,95	+0,90	−0,97	1,87	−0,25
	O1	*Oliva bulbosa*	+1,83	+0,23	1,60	+1,73	+0,83	0,90	+1,11
US70	A2	*Anadara uropigimelana*	+0,11	−1,38	1,49	+0,11	−1,38	1,49	−0,71
	T1	*Tivela stefaninii*	+1,40	+0,28	1,12	+1,24	+0,28	0,96	+0,91
US95	A1	*Anadara uropigimelana*	+0,57	−0,87	1.44	+0,57	−0,87	1.44	−0,08
	O2	*Oliva bulbosa*	+1,50	+0,77	0,73	+1,50	+0,80	0,70	+1,11

9,85 °C (*T. stefaninii*) (Fig. 8B–Table 2). The $\Delta\delta^{13}C_{as}$ and $\Delta\delta^{13}C_{oc}$ values range from 0,59 ‰ (*O. bulbosa*) to 2,68 ‰ (*T. stefaninii*) and from 0,37 ‰ (*O. bulbosa*) to 1,95 ‰ (*T. stefaninii*), respectively (Table 4).

Considering the three occupation phases we observed different patterns (Table 3): an increase of the average warmest palaeotemperatures ($T_{avg\text{-}warm}$, from 26,70 to 26,91 to 29,13 °C) and a decrease in the coldest palaeotemperatures ($T_{avg\text{-}cold}$, from 21,88 to 20,84 to 20,49 °C) from the oldest to the youngest phase, leading to an increase in seasonality (ΔT_{avg}) in both the entire shell (from 4,82 to 6,07 to 8,64 °C) and one cycle (from 3,43 to 5,54 to 8,01 °C). This increase in the seasonal palaeotemperature variation is also observable in each single species from the oldest to the youngest phase (Fig. 8, Table 2): *Anadara uropigimelana* records a ΔT_{as} from 5,04 to 5,46-7,60 to 8,90 °C and a ΔT_{oc} from 4,26 to 5,46-7,42 to 8,90 °C; *Oliva bulbosa* records the lowest ΔT: a ΔT_{as} from 4,60 to 3,87 to 5,34 °C and a ΔT_{oc} from 2,60 to 3,22 to 5,26 °C; *Tivela stefaninii* records the highest ΔT: a ΔT_{as} from 7,34 to 8,72-

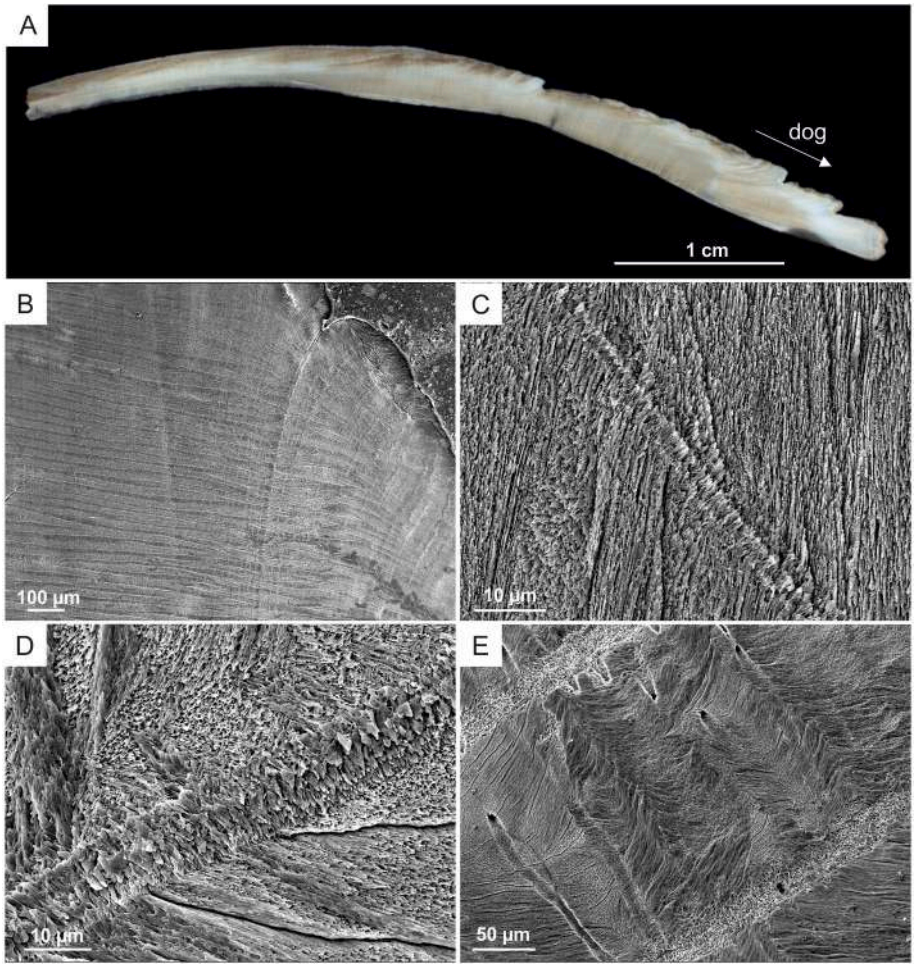

Fig. 2. A) Photo of a shell section of *Anadara uropigimelana* (specimen A3); major growth lines form steps on the outer shell surface which are traceable in the shell section; dog: direction of growth. B) Outer layer composed of crossed lamellae and dendritic nondenticular composite prisms near the outer shell surface. The growth line crosses only the linear crossed lamellar outer layer. Specimen A3 (modified from Chiari et al., 2025). C-D) Irregular simple prismatic microstructure of a major growth line in the outer crossed lamellar layer. Specimen A1 (C), specimen A4 (D, modified from Chiari et al., 2025). E) Irregular complex crossed lamellar inner layer crossed by tubules and growth lines. In the latter, the irregular simple prisms are less defined and the growth line corresponds to a band with a higher porosity. Specimen A4 (modified from Chiari et al., 2025).

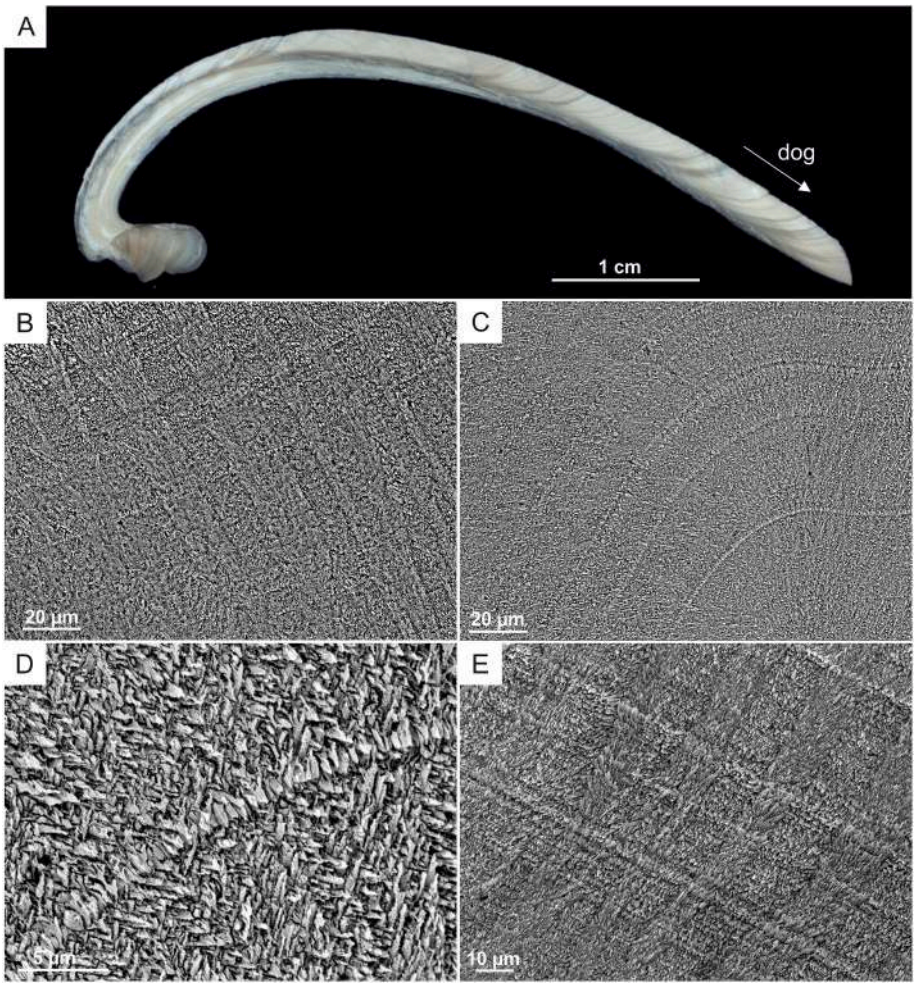

Fig. 3. A) Photo of a shell section of *Tivela stefaninii* (specimen T2); major growth lines form small steps on the outer shell surface and bundle of several growth lines form dark bands; dog: direction of growth. B, C) Numerous growth lines in the middle crossed lamellar layer. Specimen T3 (B) and Specimen T1 (C). D) Irregular simple prismatic growth line crossing the fine complex crossed lamellar inner layer. Specimen T1 (modified from Chiari et al., 2025). E) Linear crossed lamellar middle layer crossed by numerous growth lines. Specimen T2 (modified from Chiari et al., 2025).

11,59 °C and a ΔT_{oc} from 6,05 to 8,03-9,85 °C. Despite these clear trends, no particular pattern has been observed in the average palaeotemperatures considering each single species (T_{avg}) or the three phases ($T_{avg\text{-}phase}$) (Table 3).

Concerning $\delta^{13}C$ values, no trends have been observed in $\Delta\delta^{13}C_{as}$, $\Delta\delta^{13}C_{oc}$ and $\delta^{13}C_{avg}$ from the oldest to the youngest phases. *Oliva bulbosa* records the highest $\delta^{13}C_{avg}$ values (from +1,11 to +1,58 ‰), *Anadara uropigimelana* the lowest $\delta^{13}C_{avg}$ values (from −0,71 to −0,08 ‰), whereas *Tivela stefaninii* records intermediate $\delta^{13}C_{avg}$ values (from +0,59 to +1,25 ‰).

6. Discussion

6.1. Growth line formation

Most mollusc species continue to grow their calcareous shells throughout their lifespan, although the rate of growth can vary seasonally and with the ontogenetic age of the organism, typically decreasing as the animal grows older (Thomas, 2015). In all species of bivalves and gastropods which continue to grow throughout life, new growth is added incrementally at the shell edge in bivalves or aperture in gastropods. These growth increments form a chronological sequence which can preserve a detailed record of the environmental conditions experienced by the organism during its life (Thomas, 2015).

For sclerochemical methods to be successfully applied to most seasonality archives, such as mollusc shells, it is essential that the biology, especially shell growth patterns, and ecology of the species are sufficiently well understood. This knowledge is crucial for determining how seasonal variations are recorded in the archive, thereby allowing these relationships to be extrapolated to fossil or archaeological specimens (Schöne, 2008; West, 2013; Thomas, 2015; Hausmann, 2024).

Ideally, actualistic studies on living specimens should be conducted to establish a modern reference before analysing archaeological material. However, this is not always feasible, either due to the unavailability of modern reference material or because the study design did not include a preliminary investigation of the archive's seasonal dynamics. Both of these limitations apply to the present study.

While some ecological information is available for the species examined (see material section), quite nothing is known about their shell growth patterns, their timing of growth line formation or their life span. Data from congeneric species exist (e.g. Tursch et al., 1995; Sugiura et al., 2014; Marquardt et al., 2022), but they cannot be used here as a comparison as within the same genus different species can have different life spans, as well as different shell growth pattern and timing of growth line formation. In particular, no data exist for *T. stefaninii* and *O. bulbosa*. For *A. uropigimelana*, Lindauer et al. (2017) reported, in a single archaeological specimen analysed primarily for other purposes, the presence of a growth line formed during the warmest season. However, in their fig. 4 , which shows the stable isotope profile, the authors did not indicate the position of the growth line. It is also unclear

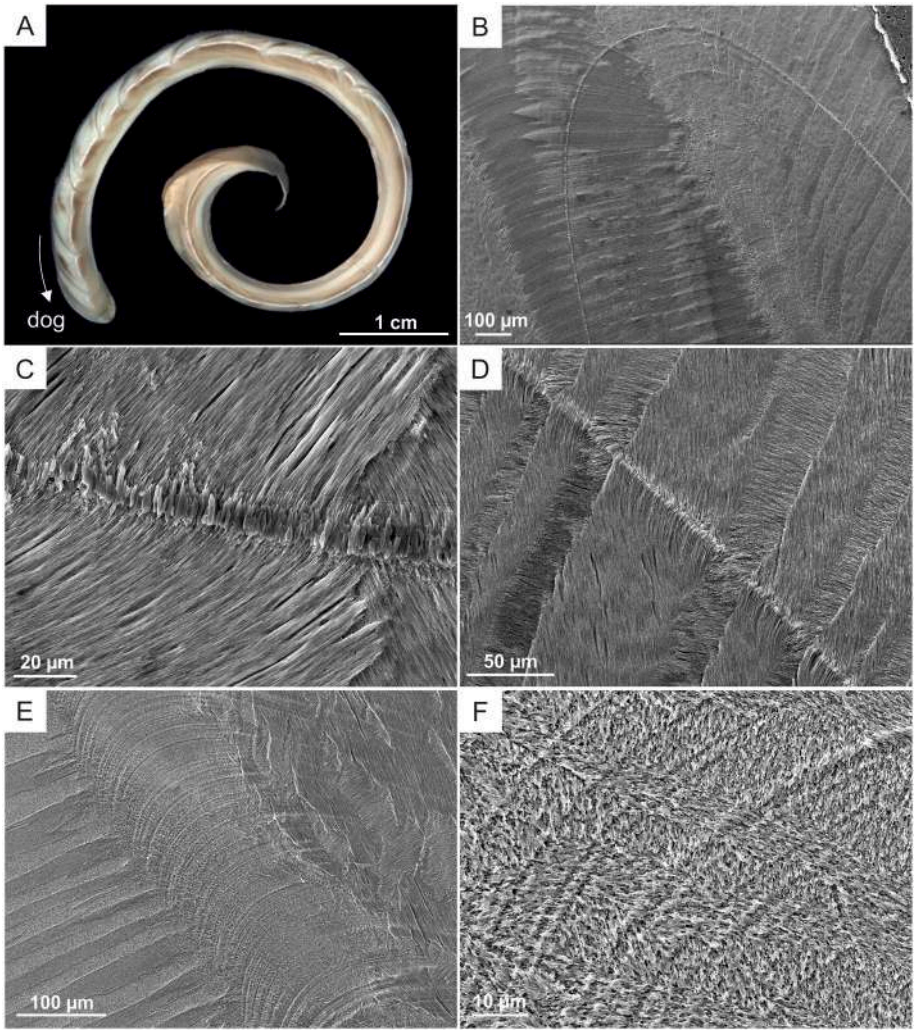

Fig. 4. A) Photo of a shell section of *Oliva bulbosa* (specimen O1); major growth lines are represented by dark curved lines crossing the entire outer and middle layer; dog: direction of growth. B) Major growth line crossing the crossed lamellar outer and middle layers and showing an irregular simple prismatic microstructure. Specimen MS-24. C, D) Growth lines in the middle layer. Specimen O2 (C) and Specimen O1 (D). E) The transitional layer, crossed by numerous tidally controlled growth lines, separates the branching crossed lamellar outer layer and the linear crossed lamellar middle layer 1. Specimen O3 (modified from Chiari et al., 2025). F) Tidally controlled growth lines crossing the branching crossed lamellar microstructure in the transitional layer. Specimen O3 (modified from Chiari et al., 2025).

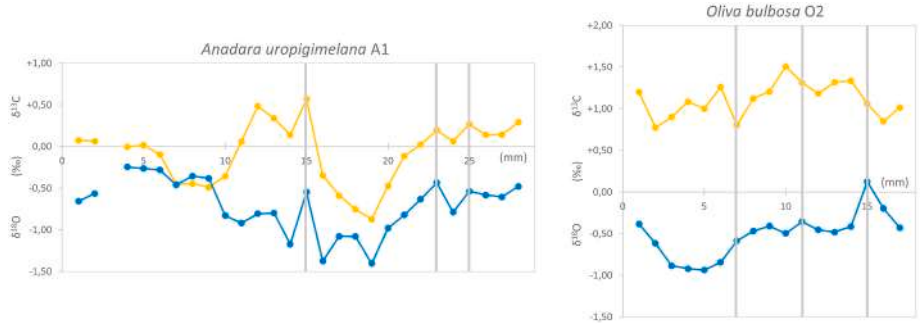

Fig. 5. $\delta^{13}C$ (yellow) and $\delta^{18}O$ (blue) data from shells of *Anadara uropigimelana* (specimen A1) and *Oliva bulbosa* (specimen O2) from the oldest occupation phase (US95; Phase 1). The position of the growth lines is represented by vertical grey bands.

whether the specimen was correctly identified as *A. uropigimelana*, as the authors frequently referred to it simply as *Anadara* sp.

Based on the isotope data obtained in the present study, the formation of annual growth lines does not occur simultaneously in the three mollusc species analysed. *Anadara uropigimelana* exhibits well-defined major growth lines, clearly visible on the outer shell surface, in polished sections, and at the SEM. In the *A. uropigimelana* specimens analysed here, annual growth lines generally correspond to the highest peaks in $\delta^{18}O$ and $\delta^{13}C$. Growth lines recording the highest $\delta^{18}O$ values indicate that, in this species, annual growth lines form during cold peaks, when water temperature is at its lowest. Indeed, specimens of *A. uropigimelana* generally record warmer temperatures compared to the

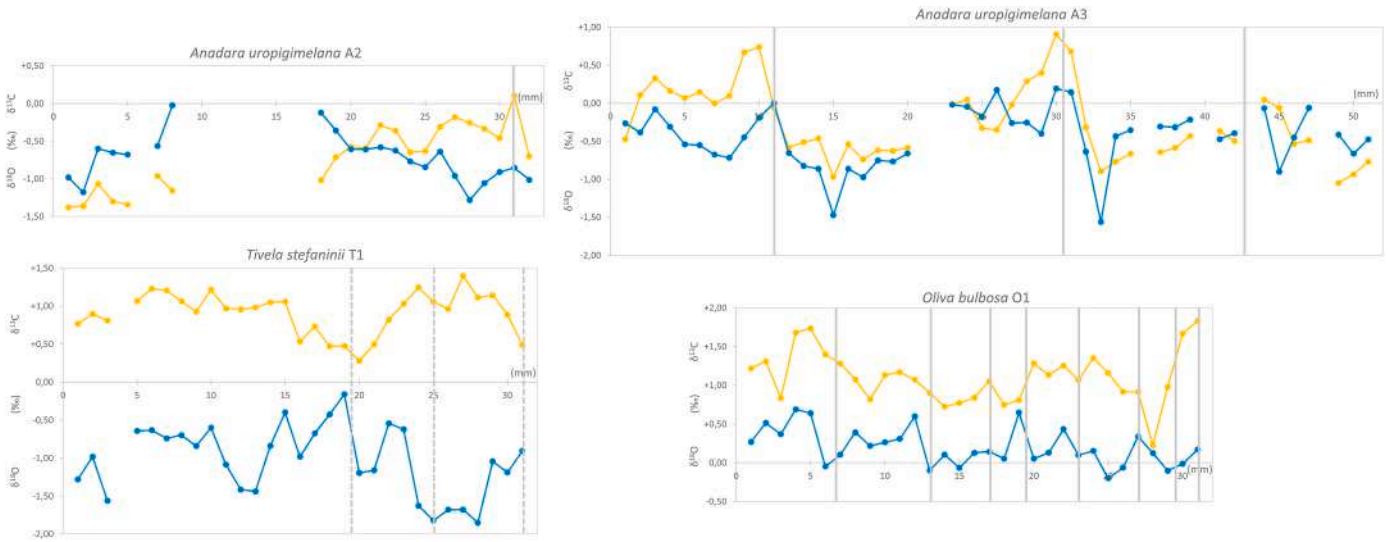

Fig. 6. $\delta^{13}C$ (yellow) and $\delta^{18}O$ (blue) data from shells of *Anadara uropigimelana* (specimens A2, A3), *Tivela stefaninii* (specimen T1) and *Oliva bulbosa* (specimen O1) from the middle occupation phase (US63, US70; Phase 2). The position of the growth lines is represented by vertical grey bands. In *Tivela stefaninii* the dashed vertical grey bands also mark growth lines; however, because they do not form visible steps on the outer shell surface, we cannot be certain that they represent major growth lines.

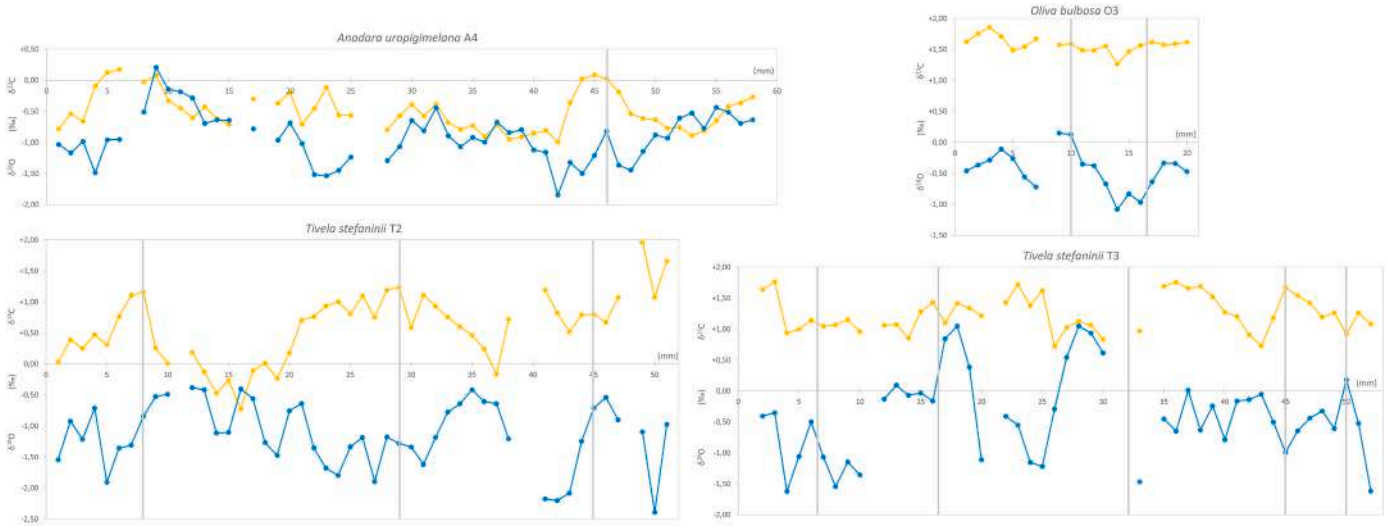

Fig. 7. $\delta^{13}C$ (yellow) and $\delta^{18}O$ (blue) data from shells of *Anadara uropigimelana* (specimen A4), *Tivela stefaninii* (specimens T2, T3) and *Oliva bulbosa* (specimen O3) from the youngest occupation phase (US30, US54; Phase 3). The position of the growth lines is represented by vertical grey bands.

other two examined species (Table 2).

Similar to *A. uropigimelana*, also *Oliva bulbosa* annual growth lines are very distinct on the outer shell surface, in polished sections, and under SEM imaging. These appear as curved, dark lines that cross the entire outer shell layer, following the curvature of the aperture. In the examined *O. bulbosa* specimens, growth lines often correspond to the lowest $\delta^{18}O$ values, with no consistent relationship to $\delta^{13}C$ values. These lower $\delta^{18}O$ values indicate that growth line formation in this species generally occurs during warmer periods, when water temperatures are higher. Indeed, specimens of *O. bulbosa* generally record the coldest temperatures and the maximum temperatures are the lowest recorded among the three species, thus confirming a reduced growth during the warmest season (Fig. 8, Table 2).

The interpretation of major growth lines in *Tivela stefaninii* is more complex, as they are less distinct compared to those in *A. uropigimelana* and *O. bulbosa*. In this study, we consider as annual growth lines those that form a step on the outer shell surface. The correlation between growth lines and isotopic profiles in the *T. stefaninii* specimens is not straightforward. Growth lines generally coincide with intermediate $\delta^{18}O$ values (i.e., between minimum and maximum values) without a clear correspondence to $\delta^{13}C$ values. This suggests that growth line formation occurs during a transitional period, specifically after the warmest season and before the onset of the coldest. This is the species generally recording the largest seasonal variation (Fig. 8, Table 2).

If on the one hand the different timing of growth line formation in the three species, slowing their growth in different seasons, may complicate the palaeoenvironmental and palaeoclimatic interpretation, on the other hand, this allows to record the full seasonal range in seawater temperatures during the examined time intervals.

6.2. Palaeoclimate during the occupation of the HAS1 site

The sclerochemical analysis performed in this study provides, for the first time, an insight into the evolution of seasonality from the oldest to

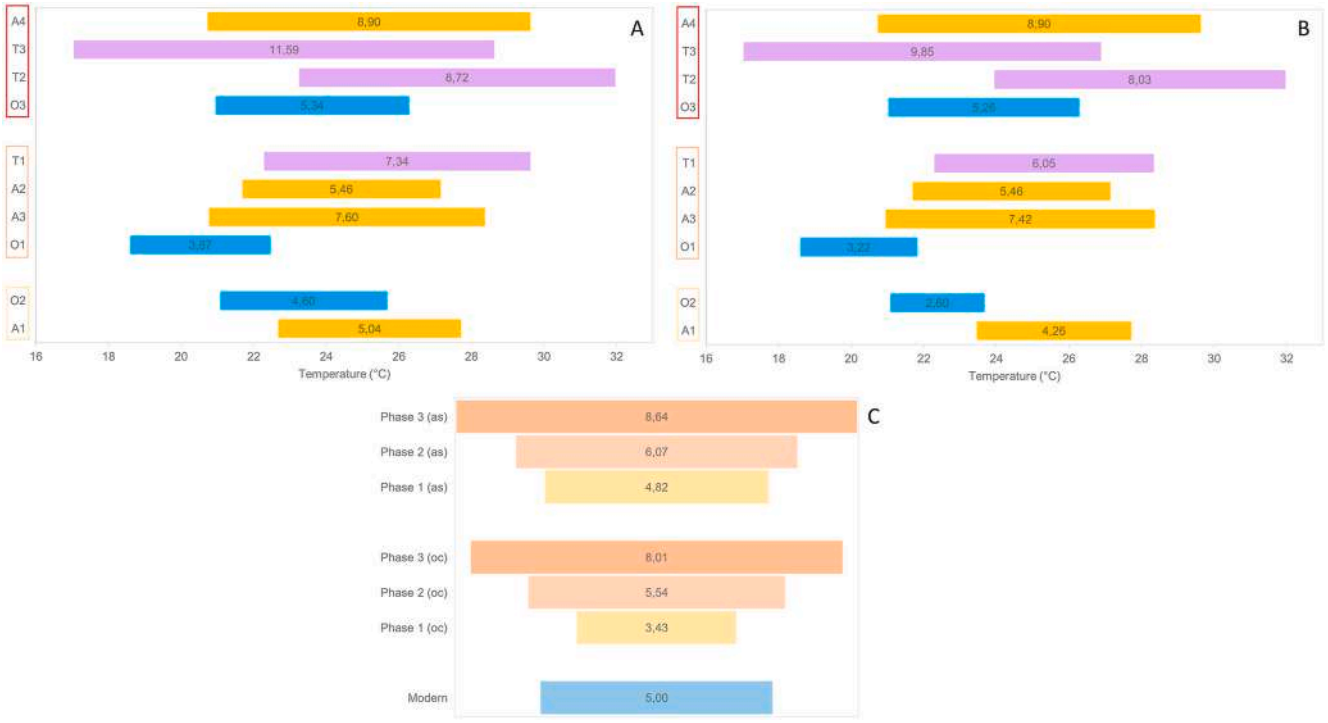

Fig. 8. A, B) Funnel charts showing the seasonal temperature variation recorded by each of the analysed specimens in all shell (A) and in one cycle (B). In yellow are represented specimens of *A. uropigimelana*, in violet those of *T. stefaninii* and in blue those of *O. bulbosa*. Coloured rectangles around specimen ID identify the three phases of site occupation: Phase 1 in yellow, Phase 2 in orange, Phase 3 in red. C) Funnel chart showing the increasing trend in seasonality from Phase 1 to Phase 3 in both all shell (as) and one cycle (oc) and modern seasonal seawater range along the coast of Salalah, Dhofar.

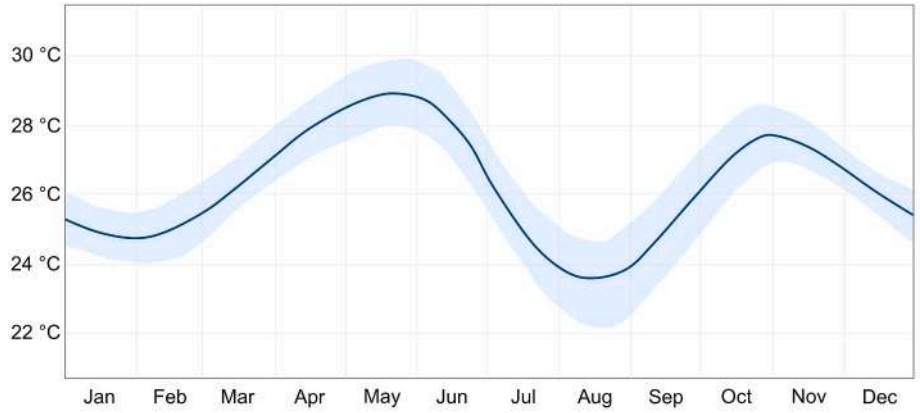

Fig. 9. Seasonal cycle of seawater temperature at Salalah. The central dark blue curve shows the multi-year mean, and the shaded light blue area represents the approximate 10th–90th percentile range of interannual variability. No additional smoothing was applied; the smooth appearance reflects averaging inherent in the underlying observational data compiled by WeatherSpark. This curve illustrates the not-classical sinusoidal annual cycle and allows estimation of the annual temperature amplitude (max–min) used for $\delta^{18}O$ interpretation (modified from weatherspark.com).

the youngest occupation phases of the Inqitat plateau by the local population. When considering the three occupation phases, a trend of increasing seasonality is observed from the oldest (Phase 1) to the youngest (Phase 3) phase, both in the seasonal signals recorded by the entire shell and by the main annual growth cycle (Fig. 8C). Although the average temperatures for each phase are similar (Table 3), the average warmest temperatures increase while the average coldest temperatures decrease, resulting in an overall enhancement of seasonality from Phase 1 to Phase 3. The same trend is evident when each species is considered individually across the three phases. It should be noted that the specimens analysed in each phase may not have lived within exactly the same time interval (i.e., they may not have been coeval), and that shell stable isotope data alone may reflect the natural isotopic variation recorded by the organism during its lifetime. Furthermore, we also acknowledge that species-specific vital effects may have influenced the different seasonal ranges recorded by different taxa. However, when these data are interpreted collectively, the increasing trend in seasonality across the three phases becomes evident (Fig. 8C).

To properly interpret these data, it is necessary to consider that the Dhofar region has a complex climatic and oceanographic setting, distinct from the rest of Oman. Modern seawater surface temperature variations along the Dhofar coast near Salalah (seasonal range: ~5 °C, Fig. 9; Prell and Streeter, 1982; Tudhope et al., 1996; Khan et al., 2021) shows that the temperature pattern deviates from the classical seasonal cycle, typically characterised by maximum annual values in summer and minimum annual values in winter. In contrast, the lowest temperatures

occur during summer, with another minimum in winter, while the highest temperatures are recorded in spring and autumn (Tudhope et al., 1996). This non-standard seasonal configuration complicates the interpretation of the isotope profiles, which do not show a typical sinusoidal curve, reflecting unique oceanographic conditions. For this reason, in our study we focus primarily on the recorded $\delta^{18}O$/temperature variations ($\Delta\delta^{18}O$ and ΔT), rather than on the specific shape of the isotope profiles.

These unusually low summer seawater temperatures are linked to the influence of the Indian Ocean monsoon acting along the Dhofar coast during summer and the consequent seasonal upwelling of Indian Ocean waters (e.g., Jung et al., 2002; Petit et al., 2007; Munz et al., 2017; Watanabe et al., 2017). Unlike the rest of Oman, the winter monsoon is weak in Dhofar, whereas the summer monsoon is stronger (Hoorn and Cremaschi, 2004; Martin, 2005; Petit et al., 2007). The alongshore monsoon winds induce coastal upwelling of cold, nutrient-rich and saline deep water to the surface, causing a decrease of seawater temperatures and an increase in salinity that occurs annually during summer months (e.g., Jung et al., 2002; Petit et al., 2007; Munz et al., 2017; Watanabe et al., 2017; Crippa et al., 2024; Müller et al., 2026). This cooling leads to the condensation and precipitation of moisture carried by the southwesterly winds on the windward side of the Dhofar Mountains (Müller et al., 2026), particularly during July and August. Due to orographic effects, most of the rainfall is concentrated on the southern slopes of the Jebel Qara, Qamar and Samhan, while the Salalah Plain receives significantly less precipitation (Khalifa, 1988). Precipitation is generally light in Dhofar mountains (daily rainfall <5 mm/day, 100-400 mm per year; Zerboni et al., 2020; Kwarteng et al., 2009; Müller et al., 2026) and occurs mainly as light rain and drizzle (Hoorn and Cremaschi, 2004; Petit et al., 2007), which consists of small droplets falling slowly and having a large specific surface area. This is a distinctive feature of the monsoon in the Dhofar Mountains, which differs markedly from the Indian Summer Monsoon in India, where rainfall can be intense with pouring rain and high precipitation rates (Müller et al., 2026). At present, the Indian Summer Monsoon contributes to groundwater recharge in the Dhofar mountains, which subsequently flows toward the Salalah coastal plain to the south and the Najd region to the north (Müller et al., 2026). The estuaries along the Salalah Plain are supplied with freshwater originating from the mountains, mainly through subsurface groundwater flow (Hoorn and Cremaschi, 2004; Zerboni et al., 2020).

Prell et al. (1992) indicated that monsoonal upwelling conditions were established around 8 Ma, when the relative abundance of endemic upwelling species of radiolarians and foraminifers increased, reflecting the onset and intensification of the modern monsoon circulation. This suggests that monsoon-driven upwelling conditions were also active during the occupation of the HAS1 settlement.

These complex oceanographic dynamics influence the stable isotope composition recorded in mollusc shells, thereby complicating the reconstruction and interpretation of palaeoclimatic and palaeoenvironmental signals and the recognition of clear annual cycles in the shells (Bemis and Geary, 1996). Upwelling and freshwater input from the summer monsoon occur during the same season (upwelling is promoted by the monsoon), but their effects tend to counteract each other: freshwater input decreases the $\delta^{18}O$ value of the seawater, while upwelling increases it. The overall impact of freshwater input on the $\delta^{18}O$ value of the seawater is probably limited, as precipitation is very low and reaches the Salalah plain mainly as subsurface groundwater flow (e.g. Zerboni et al., 2020; Müller et al., 2026). Upwelling may have amplified the coldest temperatures recorded, while minor precipitation events occurring in spring or autumn (Prell and Streeter, 1982; Kwarteng et al., 2009; Gunawardhan and Al-Rawas, 2016; Khan et al., 2021), when seawater temperatures are higher, could affect the warmest seawater temperatures recorded by the shell. However, as reported by several authors (e.g., Tudhope et al., 1996; Shahjahan et al., 2012), oceanographic cruise data indicate that modern spatial and temporal gradients in salinity off southern Oman are very small, typically less than 0,4 ‰ over lateral distances of 100-200 km and water depths of 0-100 m; seasonal differences fall within a similar range (e.g., Brock et al., 1992; Currie, 1992; Tudhope et al., 1996). Extremely low rainfall, the absence of both local and regional run-off, the narrow and open continental shelf, and the distance of our sampling site from both the Red Sea and the Persian Gulf (two potential sources of high-salinity water) likely explain this relative salinity homogeneity (Tudhope et al., 1996). Based on this evidence, changes in the oxygen isotopic composition of seawater resulting from rainfall, evaporation, or the mixing of different water masses seem to be small compared to the temperature-driven isotopic signals recorded by bivalve shells. However, seasonal variability in salinity and thus in $\delta^{18}O$ seawater value cannot be excluded, but likely contribute to the isotopic signal recorded in the shells and to the observed enhanced seasonality. As this variability cannot be constrained, its effect on reconstructed temperatures is difficult to quantify. Consequently, while salinity variations are unlikely to dominate the $\delta^{18}O$ signal, they represent an additional source of uncertainty that may influence both absolute temperature estimates and the reconstructed seasonal variability, as discussed in the following paragraphs.

Based on these premises, interesting information on the monsoon activity during the occupation phases of the site can be gained from the sclerochemistry of the analysed shells. When comparing the seasonal temperature variations inferred from the molluscs analysed in this study with modern values (seasonal range: ~5 °C, Fig. 8C and 9), we observe that seasonality was lower than today during Phase 1, comparable to present-day conditions in Phase 2, and higher than today during Phase 3.

The progressive increase in seasonality recorded by the shells may reflect a gradual strengthening of monsoon activity from the earliest to the latest occupation phases, possibly linked to enhanced upwelling of colder, more saline waters, which would have amplified the seasonal signal preserved in the shells, together with an increase in rainfall. Indeed, toward the youngest phase, we observe a decrease in the coldest temperatures, indicating more intense upwelling and thus high $\delta^{18}O$ values recorded by the shells, and an increase in the warmest temperatures, possibly reflecting more freshwater runoff and thus low $\delta^{18}O$ values recorded by the shells. These combined effects would further amplify the seasonal contrast recorded in the shells.

To identify upwelling events and quantify their intensity, Killingley and Berger (1979) proposed to use the occurrence of a negative correlation between oxygen and carbon isotope ratios in mollusc shells. Shells accreted during periods of upwelling are expected to exhibit higher $\delta^{18}O$ and lower $\delta^{13}C$ values, because upwelled waters are cool, ^{18}O-enriched, and ^{13}C-depleted, resulting in a negative $\delta^{18}O$-$\delta^{13}C$ correlation. Although this relationship has been documented in several studies (e.g., Killingley and Berger, 1979; Tao et al., 2013; Bassett and Andrus, 2021), it is not always straightforward. The $\delta^{13}C$ minima and $\delta^{18}O$ maxima are not necessarily synchronous (Killingley and Berger, 1979; Tao et al., 2013; Caldarescu et al., 2021) and the negative $\delta^{18}O$-$\delta^{13}C$ correlation, often considered diagnostic of upwelling, may not always be a reliable indicator for reconstructing such events. Bemis and Geary (1996) and Tao et al. (2013) further suggested that eutrophic environments, such as Pacific upwelling areas, are characterised by high $\Delta\delta^{18}O$ (2.3‰-3.2‰), a pattern also observed in our specimens, mainly in those from Phase 3.

In the specimens here examined, the correlation between $\delta^{18}O$ and $\delta^{13}C$ is not straightforward (Supplementary Fig. S2). *Anadara uropigimelana* specimens show both positive and negative correlation, *Tivela stefaninii* a negative, and *Oliva bulbosa* a positive correlation. To be noted that these correlations are always weak ($R^2 < 0{,}2767$ in all the specimens) and therefore not useful. When looking at the profiles in more detail, in *A. uropigimelana*, $\delta^{18}O$ peaks generally coincide with $\delta^{13}C$ peaks, indicating cold conditions associated with an enhanced productivity event (^{13}C-enriched waters). In *T. stefaninii*, especially in specimens from Phase 3, $\delta^{18}O$ peaks often correspond to low or intermediate $\delta^{13}C$ values, suggesting the upwelling of cold and nutrient-rich waters,

which are enriched in ^{12}C. The *Oliva bulbosa* profiles are comparatively flatter than those of the other two species, making it difficult to discern any clear isotopic correlation. As upwelling is also associated with increased nutrient inputs, it promotes seasonally higher primary productivity, leaving surface waters relatively enriched in ^{13}C. Consequently, in upwelling zone the $\delta^{13}C_{DIC}$ value would initially decrease before subsequently increasing (Bassett and Andrus, 2021). However, this general trend may be complicated by a desynchronization between upwelling and the resulting phytoplankton blooms (Graniero et al., 2017). This lag can be short and therefore difficult to resolve in our sclerochemical analyses. For instance, Henson and Thomas (2007) documented a 15-day delay between upwelling and phytoplankton blooms in the modern California Current system. This may explain why in some cases we observe a correlation between $\delta^{18}O$ and $\delta^{13}C$ peaks, whereas in others we do not. Such variability may reflect the fact that the three taxa do not record the same seasonal window, despite living in the same time interval, possibly documenting slightly different stages of the same upwelling event. *A. uropigimelana* primarily grows during the warm-intermediate season and slows or stops growth during the coldest months; *O. bulbosa* grows mainly during cold-intermediate seasons (growth lines forming when temperatures are higher), whereas *T. stefaninii* records both the warmest and coldest seasons (growth lines forming between the highest and lowest temperatures). For example, *T. stefaninii*, in recording the coldest season, may capture both the initial arrival of cold, nutrient-rich (^{12}C-enriched) upwelled waters and the subsequent phytoplankton bloom (^{13}C-enriched waters). In contrast, *A. uropigimelana*, which reduces growth during the coldest phase, may preferentially record the later productivity signal rather than the full upwelling cycle, resulting in different $\delta^{13}C$-$\delta^{18}O$ correlations among species living within the same interval. Besides these explanations, the different $\delta^{13}C$-$\delta^{18}O$ correlations may be also due to different living and feeding strategies (*Anadara uropigimelana* is an epifaunal/seminfaunal species, *Tivela stefaninii* is an infaunal bivalve, whereas *Oliva bulbosa* is an epifaunal gastropod). These different life habits may potentially affect their internal utilization of the dissolved organic carbon. As widely discussed in the literature, carbon isotopes in molluscs are influenced by variable contributions of metabolic CO_2 and ambient dissolved organic carbon (McConnaughey et al., 1997; McConnaughey and Gillikin, 2008). Species-specific vital effects may therefore modulate or even decouple $\delta^{13}C$ from purely environmental forcing.

Despite these complications, the shells from Phase 1 to Phase 3 record a progressive intensification of seasonal signals, suggesting enhanced monsoon activity and strengthened upwelling from the 9th BCE to 1st century CE. Geomorphological and palynological evidence from the Dhofar coastal wetlands indicates that between ca. 752–391 BCE and 250–534 CE, partly overlapping with our dataset, freshwater runoff into the estuaries was substantially greater than at present, reflecting enhanced SW summer monsoon activity (Hoorn and Cremaschi, 2004). The highly dynamic and non-linear behaviour of these estuarine systems implies strong seasonal contrasts rather than uniformly wet conditions. At Sumhuram, high-resolution palynological records document repeated short-lived flooding events between ca. 204 BCE and 130 CE, pointing to intense and concentrated rainfall episodes during a phase of stronger monsoonal influence (Mariotti Lippi et al., 2011). The event-driven and discontinuous nature of sedimentation during this interval, as highlighted by subsequent archaeopalynological reassessments (Bellini et al., 2011), further supports a climate regime characterised by pronounced intra-annual variability. Taken together, these independent terrestrial records support a context of intensified monsoon influence during the period investigated here and especially in the last occupation phase, within which the progressive strengthening of seasonal signals observed in the shells is best interpreted as an amplification of seasonal contrasts rather than a simple increase in mean annual humidity.

To our knowledge, no other coeval records with a temporal resolution comparable to that of the present study are available for assessing the evolution of monsoon activity in Dhofar. Speleothem data (Fleitmann et al., 2003, 2007) indicate a weakening of the summer monsoon during the Middle and Late Holocene, resulting in decreased precipitation. However, Kiran Kumar and Ramesh (2017) argued that there is no clear evidence for a steady decline of the South Asian summer monsoon throughout the Holocene; on the contrary, their results suggest a progressive increase in monsoon rainfall. Regardless of these different interpretations, the isotopic patterns recorded in the Khor Rori shells may represent short-term fluctuations superimposed on a longer-term climatic trend.

6.3. Impact of climatic conditions on human site occupation

The Dhofar region is a key area for understanding past human groups. Southern Oman, in fact, has long been regarded as a demographic and environmental *refugium* during earlier arid phases, sustained by monsoon-driven moisture along the Dhofar escarpment (Rose et al., 2019). From the Iron Age onwards, the same region became increasingly integrated into regional and long-distance exchange networks, initially through overland caravan routes, and later via Indian Ocean maritime routes, thanks mainly to the presence of the highest-quality frankincense (Avanzini, 2008; Newton and Zarins, 2010). Its primary export product was frankincense, a resin produced by *Boswellia sacra*, a tree growing on the Nejd plateau and in the drier wadis of the mountain ranges of southern Oman and eastern Yemen (Raffaelli et al., 2011; Hoorn and Cremaschi, 2004). Important settlements, such as the South Arabian city of Sumhuram, located near the site of Inqitat (Khor Rori archaeological park), played a crucial role within the region's trade networks during the Late Iron Age. Consequently, understanding how human adaptation and resource exploitation respond to changing environmental conditions, especially in desert environments, is essential. Environment and climate are, indeed, key variables influencing human decision-making (e.g., Twaddle et al., 2016 and reference therein).

The climatic conditions, i.e. the increase in monsoon intensity and upwelling from Phase 1 to Phase 3, indicated by the sclerochemical analysis of the shells analysed in this study may also have implications for the different patterns of site occupation by the local population. Three distinct phases of use of the promontory were identified (Lischi, 2022; Crippa et al., 2024). During the Early Iron Age (Phase 1, US95 and US98), the area was exploited with less intensity. In the Middle Iron Age (Phase 2, US63 and US70) the coastal environment experienced intensive use, corresponding to the main occupation phase of the settlement. During the Late Iron Age (Phase 3; US30 and US54), the area continued to be used with a comparable intensity; however, this phase also suggests the establishment of contacts with Sumhuram, founded around the end of the 2nd century BCE, and an increasing involvement in wider regional and international exchange networks. The final destruction of the settlement by fire (end of the 1st – beginning of the 2nd century CE), possibly intentional, may be tentatively linked to processes of territorial control associated with the emergence of Sumhuram.

An increase in monsoon activity may have positive effects on human societies, as it enhances water availability, particularly in arid regions. Conversely, decrease in precipitation and increasing aridity can contribute to population movements and migration (Gupta et al., 2006). However, excessive rainfall and prolonged summer monsoon seasons, leading to extreme climatic events such as cyclones or widespread flooding, can have detrimental effects, including severe damage to agricultural production (Gupta et al., 2006).

An intensification of the summer monsoon can also strengthen associated upwelling processes, thereby fuelling biological productivity within the euphotic zone and ultimately increasing food availability.

Upwelling brings substantial nutrient inputs to surface waters, promoting biomass development through increases in both phytoplankton and zooplankton. These planktonic blooms, in turn, attract large quantities of fish, such as sardines. The high abundance of fish in upwelling zones therefore makes these areas particularly attractive to human populations (Martin, 2005). Today, the northern Arabian Sea is regarded as one of the most productive marine regions in the world (e.g., Tudhope et al., 1996; Munz et al., 2017; Watanabe et al., 2017). However, upwelling may also contribute, together with ongoing climate warming, to the development of harmful algal blooms, which exert significant impacts on the distribution and survival of coastal marine biota (Al-Azri et al., 2012; Burt et al., 2016).

While the abandonment of the HAS1 site is archaeologically associated with its destruction by fire, most plausibly linked to deliberate actions connected with the establishment of Sumhuram, environmental factors may nevertheless have played an important indirect role during the final phases of occupation (Lischi, 2021, 2023). An intensification of summer monsoon dynamics, particularly during Phase 3, is likely to have resulted in longer and more disruptive rainy seasons, increasing the frequency and magnitude of flooding along the wadi system and placing additional stress on local infrastructures and activities. Such conditions would have required more careful management of meteoric waters, a need that is well documented within the walled city of Sumhuram through the presence of extensive water-management features (Degli Esposti and Pavan, 2020; Lischi, 2026). For the indigenous communities occupying the Inqitat plateau, prolonged monsoon seasons may have entailed extended periods of seasonal mobility towards the mountain hinterland, as strong winds, intensified rainfall, and reduced fishing opportunities would have made prolonged occupation of the coastal plateau increasingly impractical during the monsoon months.

Recent studies have shown that intensified monsoon dynamics may have had contrasting effects on coastal and inland occupations during the Iron Age. On the one hand, increased seasonality likely imposed constraints on permanent coastal habitation, particularly during the summer months, encouraging patterns of seasonal or intermittent occupation, as observed at the Iron Age Nafūn complex in south-central Oman (Danielisová et al., 2024). On the other hand, coastal environments shaped by favourable morphology, productive upwelling systems, and dynamic marine conditions would have remained highly attractive due to their exceptional availability of food and other valuable resources, supporting sustainable livelihoods despite seasonal constraints. As highlighted by Danielisová et al. (2024), the Indian Ocean coastal zone offered a rich and resilient resource base for Iron Age communities in the region. Within this broader context, it may be tentatively suggested that increased seasonal contrasts also enhanced the permeability of otherwise arid pre-desert landscapes. Given that trilith structures are widely regarded as markers of mobile pastoral practices associated with the Dhofar Inland Cultural sphere (Lischi, 2022), their eastward expansion during the Late Iron Age may have been facilitated by episodes of enhanced seasonal water availability, allowing pastoral groups to extend their seasonal mobility beyond Hadramawt and Dhofar (Garba, 2025).

7. Conclusion

Archaeological sites are often among the best sources of abundant mollusc shells from well-stratified and dated contexts. Because these shells can be directly linked to human activities, they provide a relatively straightforward means of inferring past human behaviour (Kwiecien et al., 2022), as well as the environmental conditions prevailing during human occupation (Twaddle et al., 2016). The present study represents the first sclerochemical analysis of the species *Anadara uropimigelana, Tivela stefaninii* and *Oliva bulbosa*, as well as the first application of this approach to shells from an archaeological context in Dhofar.

The main conclusions are as follows:

- Growth lines formation in the three analysed species occurred at different times: in *A. uropigimelana* growth lines form during periods of lower water temperatures, in *O. bulbosa* during periods of higher temperatures, and in *T. stefaninii* between the highest and lowest temperatures.
- Sclerochemical analyses ($\delta^{18}O$, $\delta^{13}C$) of mollusc shells reveal an increase in seasonality from Phase 1 to Phase 3 ($\Delta T_{avg\text{-}as}$ from 4,82 to 6,07 to 8,64 °C and $\Delta T_{avg\text{-}oc}$ from 3,43 to 5,54 to 8,01 °C). This enhanced seasonality may reflect stronger monsoon activity and intensified upwelling from the 9th century BCE to the 1st century CE, across an interval of approximately 1000 years.
- These high-resolution sclerochemical profiles provide valuable contributions to palaeoclimate discussions and reconstructions, particularly in complex climatic and oceanographic settings such as Dhofar, which are often understudied due to their intrinsic complexity.
- Coastal morphology, marine environmental conditions, and upwelling dynamics likely made the area surrounding the HAS1 site especially rich in food resources, rendering it highly attractive to human populations.
- The intensification of the summer monsoon, particularly during Phase 3, may have led to longer and more disruptive rainy seasons, with increased flooding along the wadi system. Rather than resulting in a reduced exploitation of the site, these conditions likely required a reorganisation of activities and a more careful management of meteoric waters, implying a shift in how the site and its surrounding landscape were used during the final occupation phase.

Taken together, these observations emphasise that the environmental dynamics documented at Khor Rori during the Late Iron Age should not be interpreted in isolation, nor as purely local phenomena. Instead, they point to a broader regional framework in which intensified seasonality and non-linear environmental responses structured human behaviour across southern Oman. Within this framework, coastal, inland, and urban communities adopted distinct yet coexisting adaptive strategies, ranging from flexible mobility and diversified land use to more formalised and engineered solutions for water management. The evidence from HAS1 thus contributes to a more nuanced understanding of how intensified climatic variability intersected with cultural traditions, mobility regimes, and emerging socio-political landscapes, shaping diverse pathways of human adaptation rather than uniform responses to environmental change.

Author contributions: CRediT

Gaia Crippa: Writing – review & editing, Writing – original draft, Formal analysis, Investigation, Conceptualization; Andrea Chiari: Writing – review & editing, Formal analysis, Investigation; Silvia Lischi: Writing – review & editing, Formal analysis; Mauro Cremaschi: Writing – review & editing, Formal analysis; Melanie J. Leng: Writing – review & editing; Formal analysis, Investigation.

Declaration of competing interest

The authors declare that they have no known competing financial interests or personal relationships that could have appeared to influence the work reported in this paper.

Acknowledgement

We would like to express our gratitude to the Ministry of Heritage and Tourism of the Sultanate of Oman and the Museum of Frankincense Land of Salalah for generously granting the DHOMIAP Project a long-term research permit and access to the materials presented in this paper, as well as for their invaluable support during our archaeological explorations in Dhofar over several years.

This work was also partly supported by the Italian Ministry for Universities and Research (MUR) through the project "Dipartimenti di Eccellenza 2023-27" (GC, AC and MC). We warmly thank two anonymous reviewers and the editor for their constructive comments and suggestions which improve the quality of the manuscript.

Appendix A. Supplementary data

Supplementary data to this article can be found online at https://doi.org/10.1016/j.quascirev.2026.109975.

Data availability

All data and/or code is contained within the submission.

References

Al-Azri, A., Piontkovski, S., Al-Hashmi, K., Al-Gheilani, H., Al-Habsi, H., Al-Khusaibi, S., Al-Azri, N., 2012. The occurrence of algal blooms in Omani coastal waters. Aquat. Ecosys. Health Manag. 15, 56–63. https://doi.org/10.1080/14634988.2012.672151.

Andrus, C.F.T., 2011. Shell midden sclerochronology. Quat. Sci. Rev. 30, 2892–2905. https://doi.org/10.1016/j.quascirev.2011.07.016.

Andrus, C.F.T., Crowe, D., 2000. Geochemical analysis of *Crassostrea virginica* as a method to determine season of capture. J. Archaeol. Sci. 27, 33–43. https://doi.org/10.1006/jasc.1999.0417.

Andrus, C.F.T., Thompson, V.D., 2012. Determining the habitats of mollusk collection at the Sapelo Island shell ring complex, Georgia, USA using oxygen isotope sclerochronology. J. Archaeol. Sci. 39, 215–228. https://doi.org/10.1016/j.jas.2011.08.002.

Avanzini, A., 2008. A Port in Arabia Between Rome and the Indian Ocean (3Rd C. BC - 5th C. AD), Khor Rori Report 2. L'Erma di Bretschneider, Roma, p. 752.

Bassett, C.N., Andrus, C.F.T., 2021. Examining the potential of Pacific abalone as a novel high-resolution archive of upwelling in the California Current. Palaeoecology 571, 110342. https://doi.org/10.1016/j.palaeo.2021.110342.

Bellini, C., Condoluci, C., Giachi, G., Gonnelli, T., Mariotti Lippi, M., 2011. Interpretative scenarios emerging from plant micro- and macroremains in the Iron Age site of Salut, Sultanate of Oman. J. Archaeol. Sci. 38, 2775–2789. https://doi.org/10.1016/j.jas.2011.06.021.

Bemis, B.E., Geary, D.H., 1996. The usefulness of bivalve stable isotope profiles as environmental indicators: data from the eastern Pacific Ocean and the southern Caribbean Sea. Palaios 11, 328–339. https://doi.org/10.2307/3515243.

Berger, J.F., Guilbert-Berger, R., Marrast, A., Munoz, O., Guy, H., Barra, A., López-Sáez, J.A., Pérez-Díaz, S., Mashkour, M., Debue, K., Lefèvre, C., Gosselin, M., Mougne, C., Bruniaux, G., Thorin, S., Nisbet, R., Oberlin, C., Mercier, N., Richard, M., Depreux, B., Perret, F., Béarez, P., 2020. First contribution of the excavation and chronostratigraphic study of the Ruways 1 Neolithic shell midden (Oman) in terms of Neolithisation, palaeoeconomy, socialenvironmental interactions and site formation processes. Arabian Archaeol. Epigr. 31, 32–49. https://doi.org/10.1111/aae.12144.

Bory de St.-Vincent, J.B.G.M., 1827. Tableau encyclopédique et méthodique des trois règnes de la nature. Vers, coquilles, mollusques et polypiers. Tome 1 (29), 83–84, 133-180.

Brock, J.C., McClain, C.R., Hay, W.W., 1992. A southwest monsoon hydrographic climatology for the northwestern Arabian Sea. J. Geophys. Res. 97, 9455–9465.

Burchell, M., Hallmann, N., Martindale, A., Cannon, A., Schöne, B.R., 2013. Seasonality and intensity of shellfish harvesting on the North Coast of British Columbia. J. I. Coast Archaeol. 8 (2), 152–169. https://doi.org/10.1080/15564894.2013.787566.

Burt, J.A., Coles, S., van Lavieren, H., Taylor, O., Looker, E., Samimi-Namin, K., 2016. Oman's coral reefs: a unique ecosystem challenged by natural and man-related stresses and in need of conservation. Mar. Pollut. Bull. 105, 498–506. https://doi.org/10.1016/j.marpolbul.2015.11.010.

Butler, P.G., Freitas, P.S., Burchell, M., Chauvaud, L., 2019. Archaeology and sclerochronology of marine bivalves. In: Smaal, A., Ferreira, J.G., Grant, J., Petersen, J.K., Strand, Ø. (Eds.), Goods and Services of Marine Bivalves. Springer, Cham, pp. 413–444. https://doi.org/10.1007/978-3-319-96776-9.

Caldarescu, D.E., Sadatzki, H., Andersson, C., Schäfer, P., Fortunato, H., Meckler, A.N., 2021. Clumped isotope thermometry in bivalve shells: a tool for reconstructing seasonal upwelling. Geochem. Cosmochim. Acta 294, 174–191. https://doi.org/10.1016/j.gca.2020.11.019.

Callapez, P.M., Dinis, P.A., 2020. Mollusc remains from the Quelba/Kalba fortification (late 16th to 18th centuries, Sharjah, UAE): taxonomical, taphonomical, environmental and cultural implications. Annual Sharjah Archaeology 17, 175–216.

Campbell, G., 2017. "What do I do with all these shells?" basic guidance for the recovery, processing and retention of archaeological marine shells. Quat. Int. 427, 13–20. https://doi.org/10.1016/j.quaint.2015.09.013.

Carenti, G., Wilkens, B., 2008. Terrestrial fauna and marine produce in Sumhuram. In: Avanzini, A. (Ed.), A Port in Arabia Between Rome and the Indian Ocean (3Rd C. BC-5th C. Ad): Khor Rori Report 2."L'Erma"di Bretschneider, Roma, pp. 477–547.

Chiari, A., Dapiaggi, M., Crippa, G., 2025. Shell microstructure and mineralogy of the mollusc species *Anadara uropigimelana* (Bory de Saint-Vincent, 1827), *Tivela stefaninii* (Nardini, 1933) and *Oliva bulbosa* (Röding, 1798). Riv. Ital. Paleontol. Stratigr. 131 (1), 63–83. https://doi.org/10.54103/2039-4942/23510.

Cremaschi, M., 1996. La via dell'incenso di Sumhuram: condizionamenti ambientali e le premesse preistoriche. Egitto e Vicino Oriente 19, 188–198.

Cremaschi, M., 2017. A geoarchaeological perspective. In: Inqitat Archaeological Mission IQM17A E IQM17B. Unpublished Report, Salalah, pp. 25–32.

Cremaschi, M., Negrino, F., 2002. The frankincense road of Sumhuram: palaeoenvironmental and prehistorical background. In: Avanzini, A. (Ed.), Khor Rori Report 1. Arabia Antica 1, Pisa, pp. 325–363.

Cremaschi, M., Perego, A., 2008. Patterns of land use and settlements in the surroundings of Sumhuram: an intensive geoarchaeological survey at Khor Rori: report of field season February 2006. In: Avanzini, A. (Ed.), A Port in Arabia Between Rome and the Indian Ocean (3Rd C. BC-5th C. Ad): Khor Rori Report 2. "L'Erma" di Bretschneider, Roma, pp. 563–607.

Crippa, G., Lischi, S., Chiari, A., Dapiaggi, M., Cremaschi, M., 2023. Discovering fire events in the HAS1 settlement on the Dhofar coast (Oman) by a multi-methodological study of mollusk shells. Quat. Res. 113, 105–121. https://doi.org/10.1017/qua.2022.62.

Crippa, G., Lischi, S., Cremaschi, M., 2024. Investigating the Upper Holocene palaeoenvironment and human subsistence strategy in the Khor Rori coastal area by studying mollusc remains from the Inqitat plateau (Dhofar, Sultanate of Oman). J. Quat. Sci. 39 (4), 608–625. https://doi.org/10.1002/jqs.3610.

Crippa, G., Ye, F., Malinverno, C., Rizzi, A., 2016. Which is the best method to prepare invertebrate shells for SEM analysis? Testing different techniques on recent and fossil brachiopods. Boll. Soc. Paleontol. Ital. 55, 111–125. https://doi.org/10.4435/BSPI.2016.11.

Culleton, B.J., Kennett, D.J., Jones, T.L., 2009. Oxygen isotope seasonality in a temperate estuarine shell midden: a case study from CA-ALA-17 on the San Francisco Bay, California. J. Archaeol. Sci. 36, 1354–1363. https://doi.org/10.1016/j.jas.2009.01.021.

Currie, R.J., 1992. Circulation and upwelling of the coast of South-East Arabia. Oceanol. Acta 15, 43–60.

Danielisová, A., Maiorano, M.P., Chlachula, D., Frenez, D., Maini, E., Daněček, D., Trubač, J., David-Cuny, H., Garba, R., 2024. The first investigation of an Iron Age shell midden in Oman: the Nafūn complex. J. Archaeol. Sci.: Report 55, 104501. https://doi.org/10.1016/j.jasrep.2024.104501.

de Winter, N.J., Tindall, J., Johnson, A.L.A., Goudsmit-Harzevoort, B., Wichern, N., Kaskes, P., Claeys, P., Huygen, F., van Leeuwen, S., Metcalfe, B., Bakker, P., Goolaerts, S., Wesselingh, F., Ziegler, M., 2024. Amplified seasonality in western Europe in a warmer world. Sci. Adv. 10, eadl6717. https://doi.org/10.1126/sciadv.adl6717.

Degli Esposti, M., Pavan, A., 2020. Water and power in South Arabia: the excavation of "Monumental Building 1" (MB1) at Sumhuram (Sultanate of Oman). Arabian Archaeol. Epigr. 31, 393–421. https://doi.org/10.1111/aae.12159.

Delaygue, G., Bard, E., Rollion, C., Jouzel, J., Stiévenard, M., Duplessy, J.C., Ganssen, G., 2001. Oxygen isotope/salinity relationship in the northern Indian Ocean. J. Geophys. Res., Oceans 106 (C3), 4565–4574.

Eerkens, J.W., Byrd, B.F., Spero, H.J., Fritschi, A.K., 2013. Stable isotope reconstructions of shellfish harvesting seasonality in an estuarine environment: implications for late Holocene San Francisco Bay settlement patterns. J. Archaeol. Sci. 40, 2014–2024. https://doi.org/10.1016/j.jas.2012.12.018.

Epstein, S., Buchsbaum, R., Lowenstam, H.A., Urey, H.C., 1953. Revised carbonate-water temperature scale. Bull. Geol. Soc. Am. 64, 1315–1326. https://doi.org/10.1130/0016-7606(1953)64[1315:RCITS]2.0.CO;2.

Fleitmann, D., Burns, S.J., Mangini, A., Mudelsee, M., Kramers, J., Villa, I., Neff, U., Al-Subbary, A.A., Buettner, A., Hippler, D., Matter, A., 2007. Holocene ITCZ and Indian monsoon dynamics recorded in stalagmites from Oman and Yemen (Socotra). Quat. Sci. Rev. 26, 170–188. https://doi.org/10.1016/j.quascirev.2006.04.012.

Fleitmann, D., Burns, S.J., Mudelsee, M., Neff, U., Kramers, J., Mangini, A., Matter, A., 2003. Holocene forcing of the Indian monsoon recorded in a stalagmite from Southern Oman. Science 300, 1737–1739. https://doi.org/10.1126/science.1083130.

Garba, R., 2025. Hinterland monuments of ancient nomads: trilith stone structures of southeastern Arabia. In: The Archaeological Heritage of Oman 15. Archaeopress Publishing Ltd, Oxford. https://doi.org/10.32028/9781805831013.

García-Escárzaga, A., Gutiérrez-Zugasti, I., González-Morales, M.R., Arrizabalaga, A., Zech, J., Roberts, P., 2020. Shell sclerochronology and stable oxygen isotope ratios from the limpet *Patella depressa* Pennant, 1777: implications for palaeoclimate reconstruction and archaeology in northern Spain. Palaeogeogr. Palaeoclimatol. Palaeoecol. 560, 110023. https://doi.org/10.1016/j.palaeo.2020.110023, 2020.

Godfrey, M., 1988. Oxygen isotope analysis: a means for determining the seasonal gathering of the Pipi (*Donax deltoides*) by Aborigines in prehistoric Australia. Archaeol. Ocean. 23, 17–22.

Graniero, L.E., Grossman, E.L., Robbins, J., Morales, J., Thompson, R., O'Dea, A., 2017. Conus Shell $\delta^{13}C$ values as proxies for $\delta^{13}C_{DIC}$ in tropical waters. Palaeogeogr.

Palaeoclimatol. Palaeoecol. 472, 119–127. https://doi.org/10.1016/j.palaeo.2017.02.007.
Grizzle, R.E., Bricelj, V.M., AlShihi, R.M., Ward, K.M., Anderson, D.M., 2018. Marine molluscs in nearshore habitats of the United Arab Emirates: decadal changes and species of public health significance. J. Coast Res. 34, 1157–1175. https://doi.org/10.2112/JCOASTRES-D-17-00119.1.
Grossman, E.L., Ku, T.L., 1986. Oxygen and carbon isotope fractionation in biogenic aragonite - temperature effects. Chem. Geol. 59, 59–74. https://doi.org/10.1016/0168-9622(86)90057-6.
Gunawardhan, L.N., Al-Rawas, G.A., 2016. A comparison of trends in extreme rainfall using 20-year data in three major cities in Oman. J. Eng. Res. 13 (2), 137–148.
Gupta, A.K., Anderson, D.M., Pandey, D.N., Singhvi, A.K., 2006. Adaptation and human migration, and evidence of agriculture coincident with changes in the Indian summer monsoon during the Holocene. Curr. Sci. 90 (8), 1082–1090.
Gutiérrez-Zugasti, I., 2011. Coastal resource intensification across the Pleistocene-Holocene transition in Northern Spain: evidence from shell size and age distributions of marine gastropods. Quat. Int. 244, 54–66. https://doi.org/10.1016/j.quaint.2011.04.040.
Gutiérrez-Zugasti, I., Andersen, S.H., Araújo, A.C., Dupont, C., Milner, N., Monge-Soares, A.M., 2011. Shell midden research in Atlantic Europe: state of the art, research problems and perspectives for the future. Quat. Int. 239, 70–85. https://doi.org/10.1016/j.quaint.2011.02.031.
Hausmann, N., 2024. A current assessment and commentary on the field of shell seasonality. Archaeol. Anthropol. Sci. 16, 154. https://doi.org/10.1007/s12520-024-02056-8.
Henson, S.A., Thomas, A.C., 2007. Interannual variability in timing of bloom initiation in the California Current System. J. Geophys. Res. 112, C08007. https://doi.org/10.1029/2006JC003960.
Hoorn, C., Cremaschi, M., 2004. Late Holocene palaeoenvironmental history of Khawr Rawri and Khawr Al Balid (Dhofar, Sultanate of Oman). Palaeogeogr. Palaeoclimatol. Palaeoecol. 213, 1–36. https://doi.org/10.1016/j.palaeo.2004.03.014.
Jones, D.S., Quitmyer, I.R., Andrus, C.F.T., 2005. Oxygen isotopic evidence for greater seasonality in Holocene shells of *Donax variabilis* from Florida. Palaeogeogr. Palaeoclimatol. Palaeoecol. 228, 96–108. https://doi.org/10.1016/j.palaeo.2005.03.046.
Jung, S.J.A., Ivanova, E., Reichart, G.J., Davies, G.R., Ganssen, G., Kroon, D., Van Hinte, J.E., 2002. Centennial-millennial-scale monsoon variations off Somalia over the last 35 Ka, in the tectonic and climatic evolution of the Arabian Sea Region, vol. 195. Geological Society Special Publications, pp. 341–352. https://doi.org/10.1144/GSL.SP.2002.195.01.18.
Kennett, D., Voorhies, B., 1995. Middle Holocene periodicities in rainfall inferred from oxygen and carbon isotopic fluctuations in prehistoric tropical estuarine mollusc shells. Archaeometry 37, 157–170. https://doi.org/10.1111/j.1475-4754.1995.tb00734.x.
Khalifa, M.I., 1988. Geological Map of Oman, 1:100,000 Sheet NE-40-9D Salalah – Explanatory Notes. Ministry of Petroleum and Minerals. Directorate General of Minerals, Muscat, Sultanate of Oman.
Khan, S., Piao, S., Khan, I.U., Xu, B., Khan, S., Ismail, M.A., Song, Y., 2021. Variability of SST and ILD in the Arabian Sea and Sea of Oman in association with the monsoon cycle. Math. Probl Eng., 9958257 https://doi.org/10.1155/2021/9958257.
Killingley, J.S., Berger, W.H., 1979. Stable isotopes in a mollusk shell: detection of upwelling events. Science 205, 186–188. https://doi.org/10.1126/science.205.4402.186.
Kim, S.T., O'Neil, J.R., Hillaire-Marcel, C., Mucci, A., 2007. Oxygen isotope fractionation between synthetic aragonite and water: influence of temperature and Mg^{2+} concentration. Geochem. Cosmochim. Acta 71 (19), 4704–4715. https://doi.org/10.1016/j.gca.2007.04.019.
Kiran Kumar, P., Ramesh, R., 2017. Revisiting reconstructed Indian monsoon rainfall variations during the last ~25 ka from planktonic foraminiferal $\delta^{18}O$ from the Eastern Arabian Sea. Quat. Int. 443, 29–38. https://doi.org/10.1016/j.quaint.2016.07.012.
Kirby, M.X., Soniat, T.M., Spero, H.J., 1998. Stable isotope sclerochronology of Pleistocene and recent oyster shells (*Crassostrea virginica*). Palaios 13, 560–569. https://doi.org/10.2307/3515347.
Kwarteng, A.Y., Dorvlo, A.S., Vijaya Kumar, G.T., 2009. Analysis of a 27-year rainfall data (1977-2003) in the Sultanate of Oman. Int. J. Climatol. 29 (4), 605.
Kwiecien, O., Braun, T., Brunello, C.F., Faulkner, P., Hausmann, N., Helle, G., Hoggarth, J.A., Ionita, M., Jazwa, C.S., Kelmelis, S., Marwan, N., Nava-Fernandez, C., Nehme, C., Opel, T., Oster, J.L., Perşoiu, A., Petrie, C., Prufer, K., Saarni, S.M., Wolf, A., Breitenbach, S.F.M., 2022. What we talk about when we talk about seasonality – a transdisciplinary review. Earth Sci. Rev. 225, 103843. https://doi.org/10.1016/j.earscirev.2021.103843.
Lindauer, S., Milano, S., Steinhof, A., Hinderer, M., 2018. Heating mollusc shells - a radiocarbon and microstructure perspective from archaeological shells recovered from Kalba, Sharjah Emirate, UAE. J. Archaeol. Sci. 21, 528–537. https://doi.org/10.1016/j.jasrep.2018.08.041.
Lindauer, S., Santos, G.M., Steinhof, A., Yousif, E., Phillips, C., Jasim, S.A., Uerpmann, H., Hinderer, M., 2017. The local marine reservoir effect at Kalba (UAE) between the Neolithic and Bronze Age: an indicator of sea level and climate changes. Quat. Geochronol. 42, 105–116. https://doi.org/10.1016/j.quageo.2017.09.003.
Lischi, S., 2018. Macroscopic analysis of the bead assemblage from the South Arabian port of Sumhuram, Oman (seasons 2000-2013). Arabian Archaeol. Epigr. 29, 65–92. https://doi.org/10.1111/aae.12106.
Lischi, S., 2020. Beads and pendants from Inqitat (Dhofar, Sultanate of Oman). Polish Archaeol. Medit. 29, 337–354. https://doi.org/10.31338/uw.2083-537X.pam29.1.16.
Lischi, S., 2021. Notes on the South Arabian occupation of Inqitat. In: Hatke, G., Ruzicka, R. (Eds.), South Arabian Long-Distance Trade in Antiquity: "Out of Arabia.". Cambridge Scholars Publishing, Newcastle upon Tyne, pp. 228–244.
Lischi, S., 2022. Settlement Dynamics and Territorial Organization in Dhofar Between the Bronze Age and Late Antiquity: Understanding the Settlement Process of the Khor Rori Area and Development of a New Regional Cultural Model. Unpublished PhD Thesis, University of Pisa, p. 615, 2 Volumes.
Lischi, S., 2023. A first definition of the dhofar coastal culture. Anci. Civil. Cult. Resour. 1, 23–38.
Lischi, S., 2026. Dhofar Coastal culture: material culture and settlement pattern in Iron Age Dhofar. In: The Archaeological Heritage of Oman, vol. 15. Archaeopress Publishing Ltd, Oxford.
Lischi, S., 2019a. Risultati preliminari delle ricerche archeologiche presso l'insediamento HAS1 di Inqitat, Dhofar (2016–2019). Egitto e Vicino Oriente 42, 119–134 [in Italian with English abstract].
Lischi, S., 2019b. Dal Paleolitico al Periodo Islamico: la storia del Dhofar attraverso lo studio archeologico dell'Inqitat/From the Paleolithic to the Islamic Period: the History of Dhofar through the archaeological study of Inqitat. In: Frenez, D., Cattani, M. (Eds.), Sognatori/Dreamers. 40 Anni di Ricerche Archeologiche Italiane in Oman/40 Years of Italian Archaeological Research in Oman. BraDypUS, Communicating Cultural Heritage, Roma, pp. 149–151.
Lombardi, A., Buffa, V., Pavan, A., 2008. Small finds. In: Avanzini, A. (Ed.), A Port in Arabia Between Rome and the Indian Ocean (3Rd C. BC-5th C. Ad): Khor Rori Report 2. L'Erma" di Bretschneider, Roma, pp. 317–476.
Lutaenko, K.A., 2011. Status of the knowledge of the IndoPacific Anadarinae (Mollusca: bivalvia). In: Lutaenko, K.A. (Ed.), Proceedings of the Workshop, Coastal Marine Biodiversity and Bioresources of Vietnam and Adjacent Areas to the South China Sea, Nha Trang, Vietnam. Vladivostok-Nha Trang. Dalnauka, pp. 95–101.
Álvarez, M., Briz Godino, I., Balbo, A., Madella, M., 2011. Shell middens as archives of past environments, human dispersal and specialized resource management. Quat. Int. 239, 1–7. https://doi.org/10.1016/j.quaint.2010.10.025.
Mannino, M.A., Spiro, B.F., Thomas, K.D., 2003. Sampling shells for seasonality: oxygen isotope analysis on shell carbonates of the intertidal gastropod *Monodonta lineata* (da Costa) from populations across its modern range and from a Mesolithic site in southern Britain. J. Archaeol. Sci. 30, 667–679. https://doi.org/10.1016/S0305-4403(02)00238-8.
Mannino, M.A., Thomas, K.D., Leng, M.J., Piperno, M., Tusa, S., Tagliacozzo, A., 2007. Marine resources in the Mesolithic and Neolithic at the Grotta dell'Uzzo (Sicily): evidence from isotope analyses of marine shells. Archaeometry 49, 117–133. https://doi.org/10.1111/j.1475-4754.2007.00291.x.
Mariotti Lippi, M., Bellini, C., Benvenuti, M., Fedi, M., 2011. Palaeoenvironmental signals in ancient urban setting: the heavy rainfall record in Sumhuram, a pre-Islamic archaeological site of Dhofar (S Oman). Holocene 21 (6), 951–965. https://doi.org/10.1177/0959683611400203.
Marquardt, A.R., Clark, N.M., Maietta, E.G., Park, S.K., Ruttenberg, B.I., 2022. Reproduction, body condition, age, and growth of a large sandy intertidal bivalve, *Tivela stultorum*. Aquat. Biol. 31, 19–30. https://doi.org/10.3354/ab00749.
Martin, C., 2005. Les malacofaunes marines archéologiques du Ja'alan (Sultanat d'Oman): un indicateur des modes de vie des populations dans leur environnement, du Néolithique à l'Âge du Bronze. Unpublished PhD thesis. Muséum National d'Histoire Naturelle 411.
McConnaughey, T.A., Burdett, J., Whelan, J.F., Paull, C.K., 1997. Carbon isotopes in biological carbonates: respiration and photosynthesis. Geochem. Cosmochim. Acta 61, 611–622. https://doi.org/10.1016/S0016-7037(96)00361-4.
McConnaughey, T.A., Gillikin, D.P., 2008. Carbon isotopes in mollusk shell carbonates. Geo Mar. Lett. 28 (5), 287–299. https://dx.doi.org/10.1007/s00367-008-0116-4.
Milner, N., 2001. At the cutting edge: using thin sectioning to determine season of death of the European oyster, *Ostrea edulis*. J. Archaeol. Sci. 28, 861–873. https://doi.org/10.1006/jasc.2000.0618.
Müller, T., van Geldern, R., Friesen, J., Schmidt, M., Said, A.B.A.B., Knöller, K., Michelsen, N., 2026. Isotopic composition ($\delta^{18}O$, $\delta^{2}H$) of the Indian Summer Monsoon in Southern Oman: A model-aided paocess interpretation. J. Hydrol.: Reg. Stud. 64, 103172. https://doi.org/10.1016/j.ejrh.2026.103172.
Munz, P.M., Steinke, S., Böll, A., Lückge, A., Groeneveld, J., Kucera, M., Schulz, H., 2017. Decadal resolution record of Oman upwelling indicates solar forcing of the Indian summer monsoon (9–6 ka). Clim. Past 13, 491–509. https://doi.org/10.5194/cp-13-491-2017, 2017.
Nardini, S., 1933. Molluschi marine e continentali del Pleistocene della Somalia. Palaeontographia Italica, 32 (1), 169–192.
Newton, L.S., Zarins, J., 2010. Preliminary results of the Dhofar archaeological survey. Proceed. Semi. Arab. Stud. 40, 247–265.
Petit, C., Fournier, M., Gunnell, Y., 2007. Tectonic and climatic controls on rift escarpments: erosion and flexural rebound of the Dhofar passive margin (Gulf of Aden, Oman). J. Geophys. Res. 112, B03406. https://doi.org/10.1029/2006JB004554.
Prell, W.L., Murray, D.W., Clemens, S.C., Anderson, D.M., 1992. Evolution and variability of the Indian Ocean summer monsoon: evidence from the western Arabian sea drilling program. Synth. Result. Sci. Drill. Ind. Ocean Geophy. Monograph Series. 70, 447–469. https://doi.org/10.1029/GM070p0447.
Prell, W.L., Streeter, H.F., 1982. Temporal and spatial patterns of monsoonal upwelling along Arabia: a modem analogue for the interpretation of Quaternary SST anomalies. J. Mar. Res. 40, 143–155.

Prendergast, A.L., Stevens, R.E., O'Connell, T.C., Fadlalak, A., Touati, M., al-Mzeine, A., Schöne, B.R., Hunt, C.O., Barker, G., 2016. Changing patterns of eastern Mediterranean shellfish exploitation in the Late Glacial and Early Holocene: oxygen isotope evidence from gastropod in Epipaleolithic to Neolithic human occupation layers at the Haua Fteah cave, Libya. Quat. Int. 407 (Part B), 80–93.

Prendergast, A.L., Stevens, R.E., 2014. Molluscs (Isotopes): analyses in environmental archaeology. In: Smith, C. (Ed.), Encyclopedia of Global Archaeology. Springer, New York, pp. 5010–5019.

Raffaelli, M., Mosti, S., Bellini, C., Mariotti Lippi, M., 2011. Dhofar, the land of frankincense. In: Avanzini, A. (Ed.), Along the Aroma and Spice Routes. the Harbour of Sumhuram, Its Territory and the Trade between the Mediterranean, Arabia and India. Bandecchi e Vivaldi, Pisa-Pontedera, pp. 17–42.

Röding, P.F., 1798. Museum Boltenianum sive Catalogus cimeliorum e tribus regnis naturæ quæ olim collegerat Joa. Fried Bolten, M. D. p. d. per XL. annos proto physicus Hamburgensis. Pars secunda continens Conchylia sive Testacea univalvia, bivalvia & multivalvia. Trapp, Hamburg, viii + 199 pp.

Roger, J., Platel, J.P., Cavelier, C., Bourdillon-de-Grissac, C., 1989. Données nouvelles sur la stratigraphie et l'histoire géologique du Dhofar (Sultanat d'Oman). Bull. Soc. Geol. Fr. 2, 265–277. https://doi.org/10.2113/gssgfbull.V.2.265.

Rose, J.I., Hilbert, Y.H., Marks, A.E., Usik, V.I., 2019. The first peoples of Oman: palaeolithic archaeology of the Nejd Plateau. In: The Archaeological Heritage of Oman 5. Archaeopress Publishing Ltd, Oxford, p. 216. https://doi.org/10.2307/j.ctvndv6nj.

Roselló-Izquierdo, E., Morales-Muñiz, A., Popov, S.V., 2005. Gihayu: a late Stone Age fishing station in the coast of Yemen. Paleorient 116–125.

Rowland, M.J., 1983. Aborigines and environment in Holocene Australia: changing paradigms. Aust. Aborig. Stud. 2, 62–77. https://search.informit.org/doi/10.3316/informit.287956493839098.

Rowland, M.J., 1999. Holocene environmental variability: have its impacts been underestimated in Australian pre-history? The Artefact. J. Archaeol. Anthropol. Society Victoria 22, 11–48. https://search.informit.org/doi/10.3316/informit.860486115034014.

Schmidt, G.A., Bigg, G.R., Rohling, E.J., 1999. Global seawater Oxygen-18 database - v1.22. https://data.giss.nasa.gov/o18data/.

Schmitt, K., Walliser, E.O., Schöne, B.R., Gey, C.J., Schimdt, C., 2022. Environmental reconstructions based on aquatic and terrestrial snails originating from the Early Bronze Age and the late islamic Period- A stable isotope case study from the Al-Khashbah archaeological Site, Sultanate of Oman. J. Archaeol. Sci.: Report 45, 103620. https://doi.org/10.1016/j.jasrep.2022.103620.

Schöne, B.R., 2008. The curse of physiology-challenges and opportunities in the interpretation of geochemical data from mollusk shells. Geo Mar. Lett. 28, 269–285. https://doi.org/10.1007/s00367-008-0114-6.

Shackleton, N.J., 1973. Oxygen isotope analysis as a means of determining season of occupation of prehistoric midden sites. Archaeometry 15, 133–141. https://doi.org/10.1111/j.1475-4754.1973.tb00082.x.

Shahjahan, Feroz, S., Saha, R., 2012. Analysis of seasonal variations of hydro-meteorological, general and particulates in sea water along the coastline of sultanate of Oman. Int. J. Eng. Res. Technol. 1 (10), 1–7. https://doi.org/10.17577/IJERTV1IS10333.

Sugiura, D., Katayama, S., Sasa, S., Sasaki, K., 2014. Age and growth of the ark shell *Scapharca broughtonii* (Bivalvia, Arcidae) in Japanese waters. J. Shellfish Res. 33 (1), 315–324. https://doi.org/10.2983/035.033.0130.

Surge, D., Lohmann, K.C., Dettman, D.L., 2001. Controls on isotopic chemistry of the American oyster, *Crassostrea virginica*: implications for growth patterns. Palaeogeogr. Palaeoclimatol. Palaeoecol. 172, 283–296. https://doi.org/10.1016/S0031-0182(01)00303-0.

Tao, K., Robbins, J., Grossman, E., O'Dea, A., 2013. Quantifying upwelling and freshening in Nearshore tropical American environments using stable isotopes in modern gastropods. Bulletin of Marine 89 (4), 815–835. https://doi.org/10.5343/bms.2012.1065.

Thomas, K.D., 2015. Molluscs emergent, Part I: themes and trends in the scientific investigation of mollusc shells as resources for archaeological research. J. Archaeol. Sci. 56, 133–140. https://doi.org/10.1016/j.jas.2015.01.024.

Tudhope, A.W., Lea, D.W., Shimmield, G.B., Chilcott, C.P., Head, S., 1996. Monsoon climate and Arabian Sea coastal upwelling recorded in massive corals from southern Oman. Palaios 11, 347–361.

Tursch, B., Ouin, J.M., Bouillon, J., 1995. On the structure of a population of *Oliva oliva* (L., 1758) in Papua New Guinea. Studies on Olividae. 22). Apex. 10, 29–38.

Tursch, B., Germain, L., 1985. Studies on Olividae. I. A morphometric approach to the Oliva problem. Indo-Malayan Zool. 2, 331–352.

Twaddle, R.W., Ulm, S., Hinton, J., Wurster, C.M., Bird, M.I., 2016. Sclerochronological analysis of archaeological mollusc assemblages: methods, applications and future prospects. Archaeol. Anthropol. Sci. 8, 359–379. https://doi.org/10.1007/s12520-015-0228-5.

Ulm, S., 2013. 'Complexity' and the Australian continental narrative: themes in the archaeology of Holocene Australia. Quat. Int. 285, 182–192. https://doi.org/10.1016/j.quaint.2012.03.046.

Watanabe, T.K., Watanabe, T., Yamazaki, A., Pfeiffer, M., Garbe-Schönberg, D., Claereboudt, M.R., 2017. Past summer upwelling events in the Gulf of Oman derived from a coral geochemical record. Sci. Rep. 7, 4568. https://doi.org/10.1038/s41598-017-04865-5.

West, C.F., 2013. Islands, coastlines, and stable isotopes: advances in archaeology and geochemistry. J. I. Coast Archaeol. 8 (2), 149–151. https://doi.org/10.1080/15564894.2013.803895.

Zerboni, A., Perego, A., Mariani, G.S., Brandolini, F., Al Kindi, M., Regattieri, E., Zanchetta, G., Borgi, F., Charpentier, V., Cremaschi, M., 2020. Geomorphology of the Jebel Qara and coastal plain of Salalah (Dhofar, southern Sultanate of Oman). J. Maps 16, 187–198. https://doi.org/10.1080/17445647.2019.1708488.